Geochemical and palynological sea-level proxies in hemipelagic sediments: A critical assessment from the Upper Cretaceous of the Czech Republic

CrossMark

Kate Olde [a], Ian Jarvis [a,*], David Uličný [b], Martin A. Pearce [c], João Trabucho-Alexandre [d,e], Stanislav Čech [f], Darren R. Gröcke [e], Jiří Laurin [b], Lilian Švábenická [f], Bruce A. Tocher [g]

[a] Kingston University London, Centre for Earth and Environmental Sciences Research, School of Geography, Geology and Environment, Kingston upon Thames KT1 2EE, UK
[b] Institute of Geophysics, Academy of Sciences of the Czech Republic, 141 31 Prague, Czech Republic
[c] Evolution Applied Ltd, 50 Mitchell Way, Upper Rissington, Cheltenham GL54 2PL, UK
[d] Durham University, Department of Earth Sciences, Durham DH1 3LE, UK
[e] Institute of Earth Sciences, Utrecht, Budapestlaan 4, 3584 CD Utrecht, Netherlands
[f] Czech Geological Survey, 118 21 Prague, Czech Republic
[g] Statoil, 2103 Citywest Blvd Ste 800, Houston TX 77042-2834, USA

A B S T R A C T

Geochemical and palynological records are presented for an expanded Turonian–Coniacian hemipelagic succession in the central Bohemian Cretaceous Basin. A high-resolution stratigraphic framework is provided by biostratigraphy and organic carbon stable-isotope ($\delta^{13}C_{org}$) chemostratigraphy. A short-term (100 kyr) sea-level curve has been derived from high-resolution transgressive/regressive maxima / shore-proximity data established from basin-wide sediment geometries. The viability of geochemical and palynological parameters as potential sea-level proxies is tested against this independently derived sea-level record. Elemental chemostratigraphy is demonstrated to offer a reliable means of identifying medium- to long-term (0.4–2.4 Myr) sea-level trends. Manganese maxima are associated with periods of high sea level, and troughs with intervals of low sea level. Falling Mn contents accompany regression and rising values transgression. Major transgressive events associated with medium-term sea-level change are marked by sharp increases in Ti/Al ratios, but short-term (100 kyr) sea-level cycles are not consistently identified. Long-term $\delta^{13}C_{org}$ variation and dinoflagellate cyst species richness are positively correlated and show similarities to the sea-level curve. Baseline trends have a cycle duration close to the 2.4 Myr long-eccentricity cycle. Dinocyst species richness closely follows short-term changes in sea level, with marked increases in dinocyst diversity coincident with most short-term flooding events. Periods of rapid sea-level rise caused an influx of a more diverse 'outer shelf' assemblage into the study area, together with the addition of shallower water species, some of which may have been transported into the central basin by hypopycnal flows. Changes in the proportion and abundance of peridinioid dinoflagellate cysts (principally *Palaeohystrichophora infusorioides*) were controlled principally by changing nutrient levels. Proximity proxies derived from geochemical and palynological data are not always consistent with the independent sea-level model. This exemplifies the need to understand all factors influencing elemental geochemical and palynological proxies before making simplistic sea level interpretations.

1. Introduction

Sea-level change represents a major driver of environmental change in the modern and ancient Earth system. The Late Cretaceous was characterised by a long-term eustatic sea-level maximum in the earliest Turonian (~93 Ma, Fig. 1) that was one of the highest sea-level stands in the Phanerozoic (Hancock and Kauffman, 1979; Haq et al., 1987; Haq and Al-Qahtani, 2005; Haq, 2014 and references therein). The early Turonian sea-level maximum was coincident with the highest ocean water temperatures in the last 110 Myr (Friedrich et al., 2012). However, despite the long-term climate optimum, superimposed higher-frequency sea-level change during the Turonian occurred within Milankovitch timescales (Fig. 1) and, debatably, was caused by glacioeustacy (Miller et al., 2003, 2005, 2011; Moriya et al., 2007; Bornemann et al., 2008; Kominz et al., 2008; Ando et al., 2009; Floegel et al., 2011; Uličný et al., 2014). The Turonian, therefore, provides an excellent opportunity to evaluate interactions between sea-level change and a wide range of palaeoenvironmental proxies within the most extreme Late Cretaceous super-greenhouse.

Lithogeochemistry, combined with lithostratigraphy and sedimentology, has been shown to provide a potential sea-level proxy in Upper
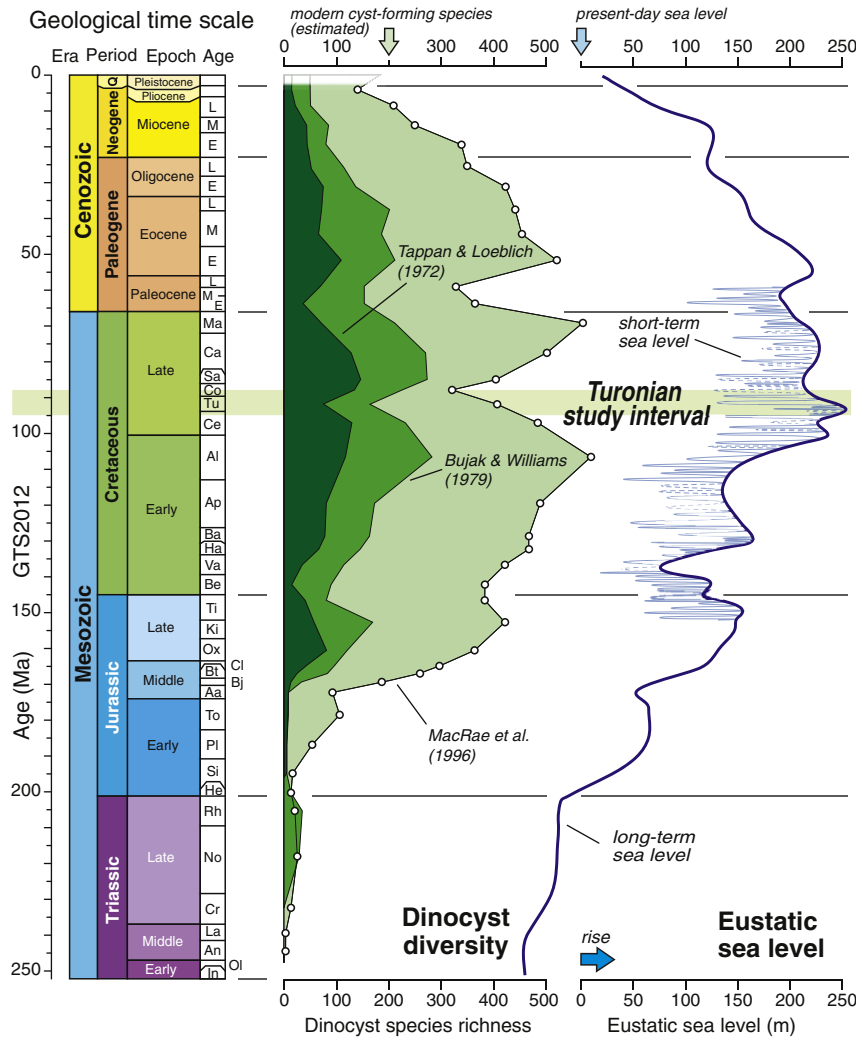
Fig. 1. Dinoflagellate cyst diversity and eustatic sea-level change through the Mesozoic–Cenozoic. Dinocyst data from Tappan and Loeblich (1972), Bujak and Williams (1979) and MacRae et al. (1996). Cretaceous short- (3rd order, pale blue) and long-term (2nd order, dark blue) sea-level curves after Haq (2014); Triassic, Jurassic and Cenozoic curve modified from Haq and Al-Qahtani (2005). All data recalibrated to the GTS2012 time scale (Gradstein et al., 2012). In, Induan; Ol, Olenekian; An, Anisian; La, Ladinian; Cr, Carnian; No, Norian; Rh, Rhaetian; He, Hettangian; Si, Sinemurian; Pl, Pliensbachian; To, Toarcian; Aa, Aalenian; Bj, Bajocian; Bt, Bathonian; Cl, Callovian; Ox, Oxfordian; Ki, Kimmeridgian; Ti, Tithonian; Be, Berriasian; Va, Valanginian; Ha, Hauterivian; Ba, Barremian; Ap, Aptian; Al, Albian; Ce, Cenomanian; Tu, Turonian; Co, Coniacian; Sa, Santonian; Ca, Campanian; Ma, Maastrichtian; Q, Quaternary. Subdivisions of the Tertiary epochs: E, Early; M, Middle; L, Late, following the age assignments of GTS2012.

Cretaceous pelagic and hemipelagic carbonate successions (e.g. Jarvis et al., 2001, 2008), enabling the recognition of stratigraphic sequences and key stratal surfaces. Increases in siliciclastic mineral associated elements such as Si, Ti, Al, Fe, and K (principally residing in quartz, clay minerals and accessory silicates), and element ratios such as Si/Al (quartz), Ti/Al (ilmenite, titanite, anatase, rutile, brookite) and Zr/Al (zircon), are indicative of elevated siliciclastic fluxes during periods of regression and lower sea level. Falling ratios are typically associated with periods of sea-level rise and highstand, with short-term maxima accompanying sediment condensation around transgressive surfaces and in maximum flooding zones. Trace elements, particularly manganese, may also show stratigraphic variation correlative to sea-level change: Mn typically exhibits minima around Exxon-type sequence boundaries and through lowstands, rising values from the transgressive surfaces through transgressive sequence tracts, maxima within maximum flooding zones, and declining values through late highstands (Corbin et al., 2000; de Rafélis et al., 2001; Jarvis et al., 2001, 2008; Renard et al., 2007).

Causal links between carbon stable-isotope fluctuations and eustatic sea-level variation have also been suggested, with a positive correlation between sea level and $\delta^{13}C$ initially being proposed based on low-resolution studies focusing on the long-term maximum flooding near

the Cenomanian–Turonian boundary (Scholle and Arthur, 1980). An underlying assumption is that an increase in organic C production and burial preferentially removes ^{12}C from the surface C reservoir, resulting in a global increase in $\delta^{13}C$ in the ocean-atmosphere system. More recent work, utilizing progressively higher-resolution datasets, has resulted in interpretations of the covariance between global sea level and carbon-isotope events (CIEs) on a Myr timescale (Gale, 1996; Mitchell et al., 1996; Jarvis et al., 2002, 2006, 2008). Conversely, other authors have argued that some positive CIEs in the Cretaceous correlate to relative sea-level falls (Gröcke et al., 2006), including those of the Middle and Late Turonian (Voigt, 2000; Wiese and Voigt, 2002), or that sea-level change cannot be invoked as the principal causal mechanism of the $\delta^{13}C$ variations (Laurin et al., 2014; Uličný et al., 2014).

Another approach that has been used to reconstruct transgressive-regressive histories and regional sea-level change in offshore facies without clear ties to coastal records, is to determine stratigraphic variation in the relative proportions of terrestrial (predominantly spores and pollen) and marine (organic-walled dinoflagellate cysts, acritarchs, foraminiferal test linings) palynomorphs. The ratio between these can be represented by the T/M index, which is assumed to be highest in more proximal (i.e. shallower water) sediments, and should decrease

in conjunction with sea-level rise (Peeters et al., 1998; Prauss, 2001, 2006). However, the ratio may be influenced by other factors, including changes in terrestrial vs. marine productivity, by climate change modulating terrestrial vegetation cover and rates of run-off, and the differential dispersion potential of spores and pollen, so additional proxy data are essential to derive reliable sea-level trends from palynological records.

Modern dinoflagellates, a major component of the phytoplankton, are most diverse in marine shelf areas and have lower diversities in oceanic and lacustrine environments; their organic walled cysts (dinocysts) are similarly most common on shelves, whereas in oceanic waters the predominant cysts are calcareous (e.g. Dale, 1992). Species richness of gonyaulacoid cysts (considered to represent phototrophic dinoflagellates), in particular, is generally highest in offshore shelf environments (Harland, 1973). Modern middle- to outer-shelf facies also have the highest abundances of dinocysts, while estuarine, inner-shelf and slope to basin areas have lower abundances (Wall et al., 1977; Bradford and Wall, 1984).

Variation in dinocyst species richness through time, since their first appearance in the Triassic, shows a strong positive correlation with eustatic sea level (Fig. 1), with highest diversities occurring during periods of high sea level and large shelf-sea areas (MacRae et al., 1996; Sluijs et al., 2005). The Upper Cretaceous exhibits the largest species numbers (>500) in the geological record, coincident with the highest eustatic sea levels. The Turonian–Coniacian interval represents a period of generally declining diversity accompanying a period of long-term sea-level fall (Fig. 1).

Previous studies of Cretaceous successions (e.g. Schiøler et al., 1997; Helenes and Somoza, 1999) have concentrated on the relative abundances and diversity of different palynological groups. Higher relative abundances of terrestrial palynomorphs are considered to indicate high terrestrial input. A high proportion of acritarchs relative to dinocysts is thought to reflect more marginal environments, whereas the highest diversity and highest abundance of dinocysts is found in offshore marine sediments.

Fossil dinocyst diversity and abundance variation have been studied in relation to sequence stratigraphy in several areas, including the Cretaceous-Palaeogene of Alabama (Habib et al., 1992), the Upper Cretaceous of SE France (Monteil, 1993), the lower Oligocene of Belgium (Stover and Hardenbol, 1994) and the upper Albian of NW Germany (Prauss, 2001). In terms of the tripartite systems tract schemes used in the 1990s, the observed trends may be summarised as follows: lowstand systems tract (LST), low species diversity; transgressive systems tract (TST), increased species diversity and abundance; highstand systems tract (HST), maximum species diversity and abundance in maximum flooding zones (MFZ), followed by a decrease in the upper part of the HST (and falling stage systems tract, FSST, of more recent sequence stratigraphic schemes; Catuneanu et al., 2011).

Prauss (1993) introduced the concept of 'sequence palynology', and compared palynological results to lithological and sedimentological features of selected Mesozoic sections. In this and subsequent investigations (Prauss, 1996, 2000, 2001), terrestrial palynomorphs abundances were shown to be highest in intervals of falling and low sea level (FSST, LST) and lowest during periods of rapid sea-level rise (TST), with dinocysts showing the opposite abundance trends. Sediments immediately above sequence boundaries (SB; i.e. base LST) displayed low numbers of dinocysts but peaks in acritarchs and prasinophyte abundance. Peaks in acritarch abundance were also noted above transgressive surfaces (TS; i.e. base TST). Numbers of dinocysts compared to other marine palynomorphs (prasinophytes, acritarchs) increased in sediments during transgression (TST), with broad maxima accompanying maximum flooding, and falling values through the late HST or FSST. Increased numbers of prasinophytes and fewer dinocysts characterised sediments above maximum flooding surfaces (MFS) or in maximum flooding zones (MFZ). Finally, trilete spores showed higher relative abundances than bisaccate pollen in sediments with greater fluvial

input, because the latter are more readily transported by wind. This difference was explained by the contrasting hydrodynamic properties of the two groups. Prauss (1993, 2000, 2001) regarded palynological trends as being caused principally by changes in hydrodynamic stability, salinity and nutrient availability.

Dinocysts may be used to infer palaeoproductivity by comparing the relative abundances of (P) and gonyaulacoid (G) cysts (P/G ratio, e.g. Lewis et al., 1990; Powell et al., 1990; Pearce et al., 2009). Whereas the dinoflagellates that form G-cysts are photosynthetic autotrophs, most peridinioid cysts are thought to have derived from heterotrophic dinoflagellates and, as pointed out by Pearce et al. (2009), although the inevitable inclusion of peridinioid cysts from phototrophic dinoflagellate species in such a ratio will modify the palaeoenvironmental signal, it is unlikely to obscure it. Modern peridinioid cysts have been documented in high abundance in less stable, high-nutrient environments, and are prominent in contemporary upwelling zones (e.g. Peruvian upwelling system, Rojas de Mandiola, 1981; Cape Blanc, Susek et al., 2005), in cold water/high-latitude nutrient-rich environments (e.g. Arctic Ocean, Mudie and Aksu, 1984; Weddell Sea, Garrison et al., 1991), and in inner shelf habitats (Bint, 1988; de Vernal and Mudie, 1989). Due to the domination of few species that are able to rapidly utilise nutrients, dinocyst species richness may be inversely proportional to nutrient availability (Valentine, 1973).

In this paper, elemental and isotopic profiles, and palynological assemblage data are compared to a tightly constrained relative sea-level history derived from transgressive-regressive trends within a European Cretaceous basin with a well-characterised sedimentary system and tight biostratigraphic framework (Uličný et al., 2014, updated herein). The basin offers an outstanding opportunity to rigorously test relationships between chemostratigraphy, palynology, sea level and palaeoenvironmental change.

2. Material and methods

2.1. Bohemian Cretaceous Basin

The Bohemian Cretaceous Basin was an intra-continental basin formed during the Cenomanian–Santonian (101–84 Ma) as a seaway between the Boreal Sea and Penninic Ocean (Fig. 2). The basin originated by the reactivation of a fault system in the Variscan basement of the Bohemian Massif, and combined features of an epeiric sea formed during global transgression with those of a tectonically active setting that contains probably the highest proportion of siliciclastics of all the European Cretaceous basins north of the Alps (Uličný et al., 2009). During Turonian–Coniacian time, fill of the Bohemian Basin was dominated by the repeated progradation of coarse-grained deltas and adjoining shorefaces, and was affected by redistribution of siliciclastics by strong along-shore tidal currents (Uličný, 2001; Mitchell et al., 2010). A maximum water depth of around ~100 m is estimated for the basin interior.

A transgressive-regressive history of the Bohemian Cretaceous Basin has been derived from the analysis of a basin-scale correlation grid, developed using well-log data (gamma-ray, resistivity, neutron porosity logs) from around >700 boreholes, in most cases supplemented by either archive descriptions of cores or study of cores and, where possible, calibrated by outcrop sedimentology and gamma-ray logging (Uličný et al., 2009, 2014). Deposition in the basin has been split into a number of genetic sequences, here termed TUR1–TUR7, CON1 and CON2, their boundaries defined by maximum transgressive surfaces / zones, which were detailed by Uličný et al. (2009). The sequences record long-term cycles of regression and subsequent transgression, within which there are multiple smaller scale events.

2.2. Běchary-1 reference core: lithofacies and depositional history

During 2010, a 405 m research core, Bch-1, was drilled through a representative Upper Cenomanian to Lower Coniacian succession of
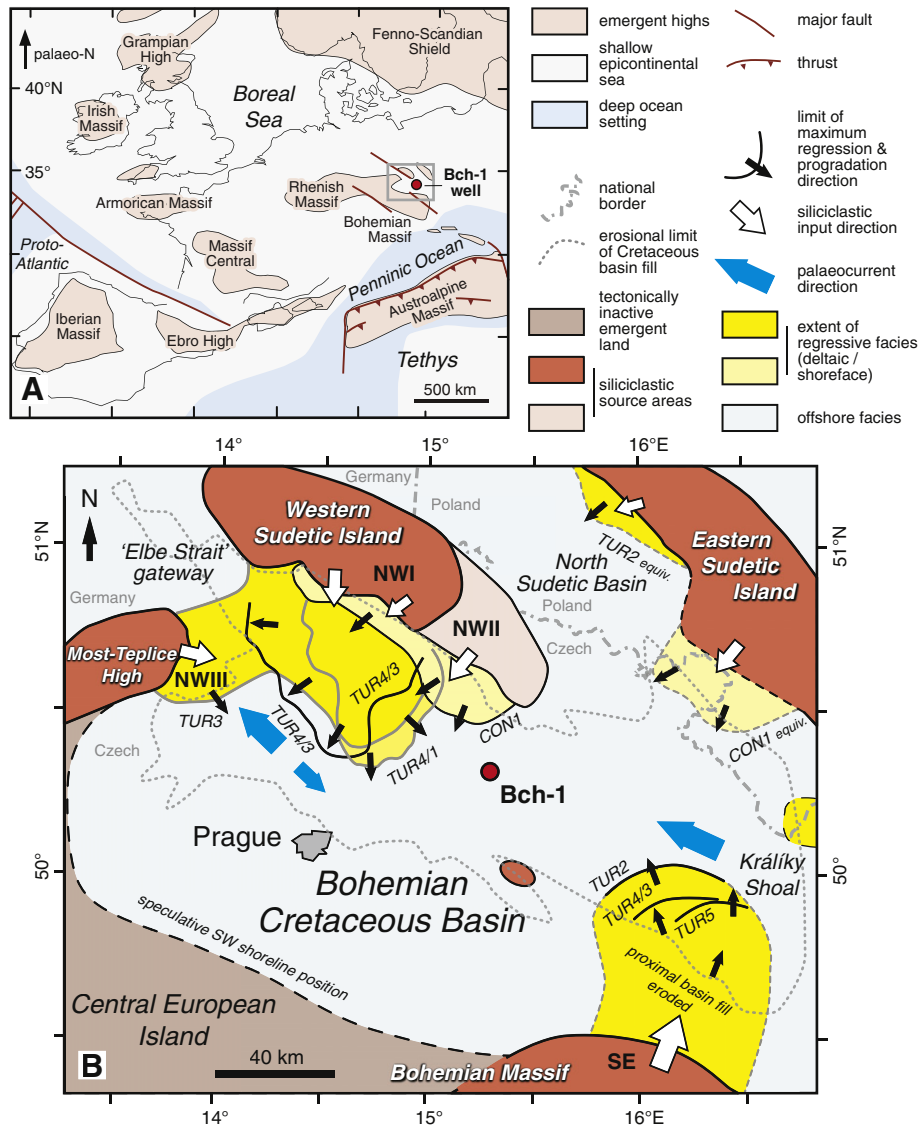
Fig. 2. Location and Turonian palaeogeography of the Bohemian Cretaceous Basin study section. (A) Simplified palaeogeography of the European epicontinental sea showing the location of the Bch-1 well. (B) Detail of the Bohemian Cretaceous Basin, location shown by rectangle in A. Main siliciclastic source areas and sub-basins are shown: NW, Lužice-Jizera sub-basin; SE, Orlice-Žďár sub-basin. TUR2–CON1 indicate regressive limits of nearshore strata in genetic sequences. Adapted from Uličný et al. (2014).

offshore marine sediments to investigate the responses of multiple proxies to sea-level change (Uličný et al., 2014). The Bch-1 site (50.31506°N 15.29497°E), located in the village of Běchary, east-central Czech Republic, is situated in the central basin between two depocentres, one adjacent to the Most-Teplice High and Western Sudetic Island in the northwest, the other bordering the emerged central part of the Bohemian Massif in the southeast (Fig. 2). These source areas contributed varying proportions of sediment through the study interval. In the current work, results obtained from detailed palynological and geochemical analysis of the Bch-1 core are compared to previously published transgressive–regressive (T–R) curves from the NW and SE depocentres and the interpreted sea-level history of the basin based on stratal geometry (Uličný et al., 2014).

The dominant lithofacies in the Bch-1 core (Fig. 3) consists of very dark grey marlstones and calcareous mudstones with a varying proportion of quartz silt; coarser muds characterise the intervals 360–380 m and 140–220 m. The mean percentage of $CaCO_3$ through the core is ~ 35%, and carbonate is generally represented by a micritic component, some mm-scale bioclasts, and recrystallised spar in horizons with concretionary cement. Total organic carbon contents

(TOC) average 0.42%. Turonian lithofacies show abundant bioturbation throughout the core, dominated by a distal *Cruziana* ichnofacies (MacEachern et al., 2010).

The Cenomanian–Turonian Boundary (CTB) near the base of the core (402 m) is marked by an omission surface. A major hiatus at this level (Uličný et al., 1993, 2014; Čech et al., 2005) is confirmed by the absence of calcareous nannofossil zones UC 5a–b of Burnett et al. (1998), which correlates to the upper part of the *M. geslinianum* and *N. juddii* ammonite zones. This hiatus has been attributed to a major flooding episode (Valečka and Skoček, 1991).

During the Early to Middle Turonian in the NW sub-basin, deltaic systems prograded to the SW from the Western Sudetic Island, and eastwards from the Most-Teplice palaeohigh (Figs. 2, 3), forming a major siliciclastic wedge that extended to the SE obliquely along the basin axis (Uličný et al., 2009). In the SE sub-basin, a major prograding wedge containing a number of stacked, thin sandstone units comprise sequences TUR1–2. The first occurrence (FO) of the ammonite *Collignoceras woollgari* (Mantell), which marks the base of the Middle Turonian, appears near the base of an LST in TUR2 in both sub-basins, and is correlated to 374 m in Bch-1 (Uličný et al., 2014).
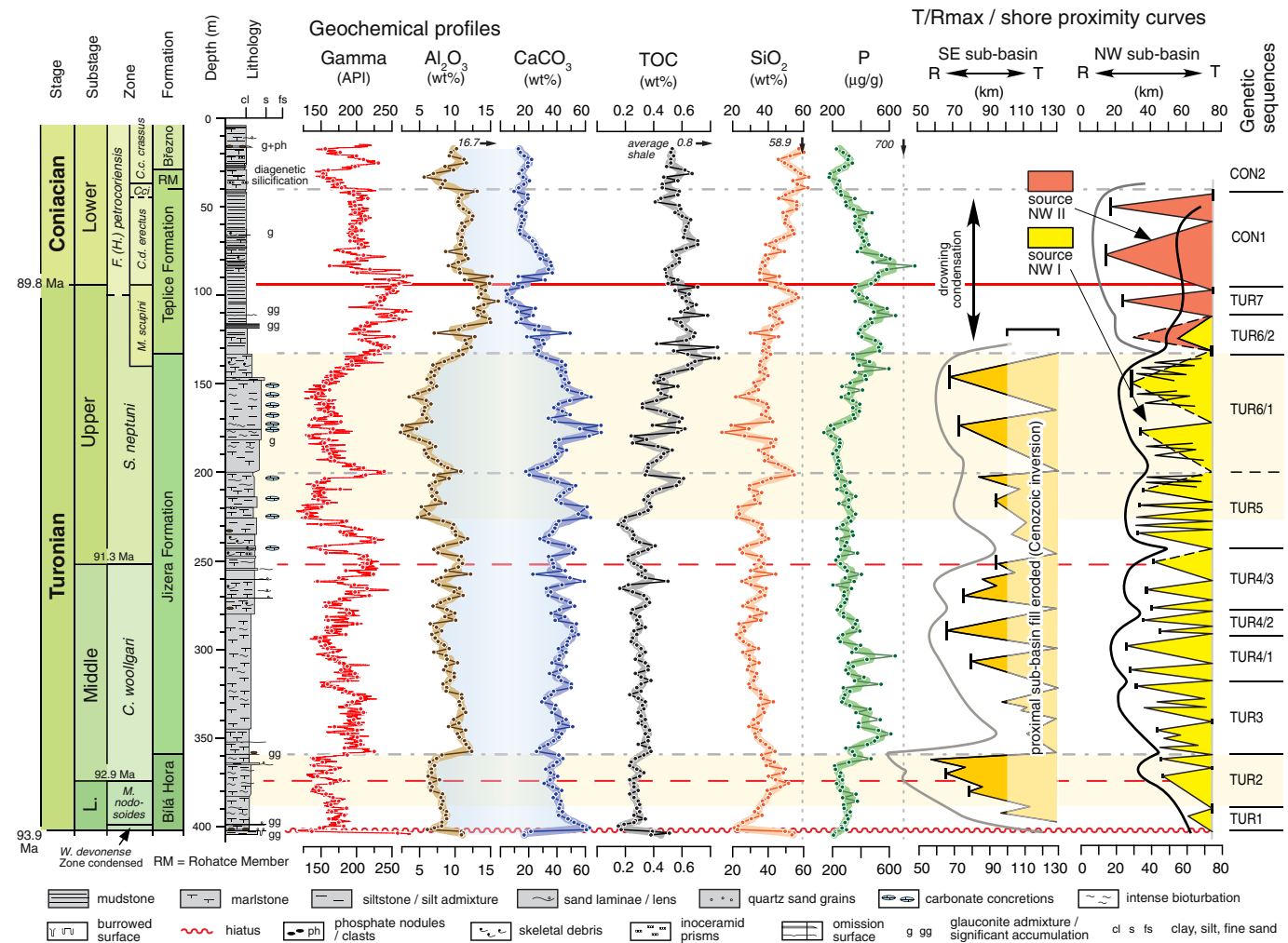
Fig. 3. Lithology and geochemical characteristics of the Bch-1 well, showing gamma ray, Al_2O_3, $CaCO_3$, total organic carbon (TOC), SiO_2 and P profiles. Ages of stage and substage boundaries derived from Ogg et al. (2012), Laurin et al. (2014) and Sageman et al. (2014). Lithostratigraphic terminology after Čech et al. (1980). Transgressive-regressive (T/Rmax / shore proximity) curves from the SE and NW depocentres (Fig. 2) and basin-scale genetic sequences are also shown (modified from Uličný et al., 2014). Pale yellow bands (TUR2; mid-TUR5 to top TUR6/1) are major regressive packages defined by geochemical data (low gamma ray, low Al and Mn; high Si/Al, Ti/Al, Zr/Al, see Fig. 5).

A significant difference in the transgressive-regressive history between the NW and SE sub-basins is observed in early Middle Turonian Sequence TUR3, where the entire SE depocentre was rapidly drowned, coincident with a regionally developed marker bed rich in glauconite and phosphate (at 359.3 m in Bch-1, Fig. 3). Due to increased basin-wide accommodation towards the end of the Middle Turonian, deposition of TUR4 extended as a package of deltaic clastics and correlative offshore fines, of relatively uniform thickness over the entire NW sub-basin. Sequence TUR4 is characterised by a series of vertically-stacked, high-frequency sub-sequences showing progradation of coarse-grained deltaic lobes in varying directions (numbered 4/1–4/3). TUR4/1 prograded mainly towards the Bch-1 site from the NW, while TUR4/3 prograded mainly towards the SW (Fig. 2; Uličný et al., 2009).

The style of deposition in Late Turonian TUR5 indicates a further increase in the long-term accommodation/supply ratio throughout the basin. The transgressive event at the base of TUR5 (245 m in Bch-1, Fig. 3) is prominent basin-wide, and marks the onset of higher carbonate contents and more widespread cementation in all facies. This transgressive event correlates to an acme of *Inoceramus perplexus* Whitfield. The coarsening-upwards trend of TUR6/1 shows increased shallowing and a progression to relatively high-energy conditions.

Coarser siliciclastic sediments of uppermost Turonian sequences TUR6/2 and TUR7 are confined mainly to a tectonically deepened marginal part of the NW sub-basin, and were sourced from both rejuvenated

and newly emerging uplifts along the Lužice Fault Zone on the western margin of the Western Sudetic Island (Uličný et al., 2009). The top of TUR6/2 is an omission surface (111 m) coincident with *Didymotis* Event 1, a Europe-wide marker bed defined by a flood of distinctive bivalves.

Turonian–Coniacian boundary Sequence CON1 is marked by lower carbonate contents (Fig. 3). The FO of *Cremnoceramus deformis erectus* (Meek), the base Coniacian marker, is found within Sequence CON1, correlated to 94 m in the Bch-1 core. The emergence of a new uplift at the eastern edge of the Western Sudetic Island during the Early Coniacian shifted the source of siliciclastics closer to the Bch-1 site (Fig. 2). From the new source area, steep-faced Gilbert-type deltas prograded into water up to 100 m deep (Uličný et al., 2009), trapping sediment in the proximal area; as a result, despite a marked increase in shore proximity in the T/R curve at this level (Fig. 3), no coincident increase in grain size is noted in the core.

2.3. Analytical methods

Samples of approximately 50 g were taken every 2 m through the 405 m Bch-1 core for elemental, isotopic and palynological analysis (196 samples). Based on an average compacted sedimentation rate for the Middle and Upper Turonian of 9 cm/kyr (Uličný et al., 2014) sampling resolution was on the order of 22 kyr. Additionally, smaller

samples (20 g, total 610) were obtained at 0.5 m (5.6 kyr resolution) intervals for carbon stable-isotope analysis of the organic fraction ($\delta^{13}C_{org}$). Samples were cleaned, chipped to < 3 mm, and homogenised. For isotopic and elemental analysis, 20 g of chips were pulverized to a fine powder in an agate mill.

For determination of elemental concentrations, 0.250 g of dried powders and 1.25 g of lithium metaborate ($LiBO_3$) flux were mixed into graphite crucibles, and fused at 1050 °C in a muffle furnace, following the method of Jarvis (2003). The resulting melts were dissolved in 0.5 M nitric acid (HNO_3), passed through filter paper (Whatman Number 41) to remove any trace of graphite. High-purity deionised water (18MΩ) was then added to the solutions so that the final solution was 0.3 M HNO_3. Analyses were performed by inductively coupled plasma - atomic emission spectroscopy (ICP-AES) employing a JY Ultima 2C spectrometer at Kingston University London. The instrument was calibrated before each analytical run using a series of in-house chalk standards. The international reference material W-2 diorite (USGS, 1995b) was run after every 5 samples to monitor instrumental drift; six other reference materials (AGV-2 andesite, CCH-1, JLs-1 limestones, MAG-1 marine mud, SCo-1, SGR-1 shales; Roelandts and Duchesne, 1994; USGS, 1995a, c, 1998, 2001; Imai et al., 1996) were run before and after every run of sample solutions. Samples were run 2 or 3 times, depending on the drift monitor stability, and mean values calculated following drift correction. Systematic bias was assessed using the SRM results and, where judged necessary, corrected in the final sample data.

$CaCO_3$ values were calculated from total Ca contents assuming that Ca resides principally in the carbonate fraction. The contribution of non-carbonate Ca was removed using values calculated from Al contents using the Ca:Al ratio for average shale of 0.178 (Wedepohl, 1971). By reference to international reference materials run with samples, accuracy and precision for major elements were judged to be <3%. Numerical data are presented in Appendix B.

For $\delta^{13}C_{org}$ determination, 5–10 ml of sample powder was reacted with 50 ml 3M HCl at room temperature for 12 hours in a centrifuge tube. Sample tubes were shaken intermittently to ensure complete reaction. Insoluble residues were rinsed four times in deionised water and dried at 50 °C. Dried residues were reground and homogenized in an agate mortar and transferred to glass vials.

Organic carbon isotope ($\delta^{13}C_{org}$) measurements were performed on 2.5–3 mg splits of the insoluble residues at Durham University using a Costech ESC4010 Elemental Analyser (EA) connected to a ThermoFinnigan Delta V Advantage isotope ratio mass spectrometer (IRMS) via a Conflo 3 interface. Up to 8 international and internal standards were analysed throughout the generation of each isotopic data set. Total organic carbon (TOC) was obtained from the mass area of CO_2 produced in the EA and determined in the IRMS. TOC was calculated using a k-factor generated from an internal standard, glutamic acid (C = 40.82%). TOC was recalculated for whole-rock TOC using $CaCO_3$ values calculated from Ca data determined by ICP-AES. Reproducibility of replicate samples was on average better than 0.2 ‰ for $\delta^{13}C_{org}$ (VPDB) and 0.04 wt% for TOC in the insoluble residue.

Splits (10 g) of chipped samples were processed for quantitative palynological analysis. Palynomorphs >15 μm were concentrated by the commercial processing company (PLS Ltd, Holyhead, UK) using the HCl-HF method of Lignum (2009), modified from Lignum et al. (2008), 'Company B' methodology. All samples were spiked with tablets containing the modern spore *Lycopodium* to allow statistically valid quantitative analysis (palynomorphs per gram, ppg). Lithological variation may cause bias in dinocyst abundances due to varying carbonate dilution (Pross et al., 2006; Pearce et al., 2009). Accordingly, ppg values were recalculated on a carbonate-free basis using $CaCO_3$ values derived from elemental Ca data.

Palynomorph identification and counting was undertaken using a Leitz Laborlux S light microscope with a 40x objective. Three hundred dinocysts were identified per sample. Broken or partial specimens were added to the count only if there was more than half of the specimen present. Unidentifiable specimens were recorded as 'indeterminate', and were not included in the count of 300, but were included when calculating total palynomorphs per gram. Following this count, the remainder of the slide was scanned to identify any additional species, which were marked as 'present', but in abundances too low to be recorded among the 300.

Numbers of other palynomorphs, including pollen, spores, acritarchs and foraminiferal test linings, were also counted. To assess the relative contribution of terrestrial material to the palynomorph assemblage, the terrestrial/marine palynomorph (T/M) index, I = t/(m + t), with t = number of terrestrial palynomorphs (spores and pollen) and m = number of marine palynomorphs (dinocysts and acritarchs), was calculated (Pross, 2001).

3. Results

3.1. Elemental geochemistry

Selected lithogeochemical profiles are shown in Fig. 3. Stratigraphic variation is dominated by three major constituents: SiO_2, ranging from 14–63 wt%; Al_2O_3, ranging from 2–16 wt%; and $CaCO_3$ ranging from 4–71 wt%. Aluminium shows an identical profile to, and correlates very strongly with, other typically clay mineral-associated elements (principally Fe, Mg, K, not shown; $R^2 > 0.8$), and the downhole gamma-ray curve ($R^2 = 0.7$). Comparison between the high-resolution (5 cm nominal; 550 yr) wireline gamma-ray data and sample results at 2-m resolution (Fig. 3; 22 kyr) demonstrates that despite its lower resolution, the bulk-rock sample data capture all significant medium- to long-term shifts (≥100 kyr) and high-amplitude geochemical variation in the section.

Calcium (and Sr) displays a near mirror-image profile to both Si and Al (Fig. 3). However, the poor correlation between Si and Al ($R^2 = 0.2$) indicates the presence of an independently varying quartz (detrital and biogenic) component, confirming that Bch-1 sediments consist principally of varying proportions of carbonate, clay minerals and quartz. This is exemplified by an Al_2O_3-SiO_2-CaO ternary plot (Fig. 4) that shows the majority of samples falling close to a mixing line between average shale and carbonate, but with scatter induced mainly by varying detrital quartz (Sequences TUR 2 and TUR5–6/1) and biogenic
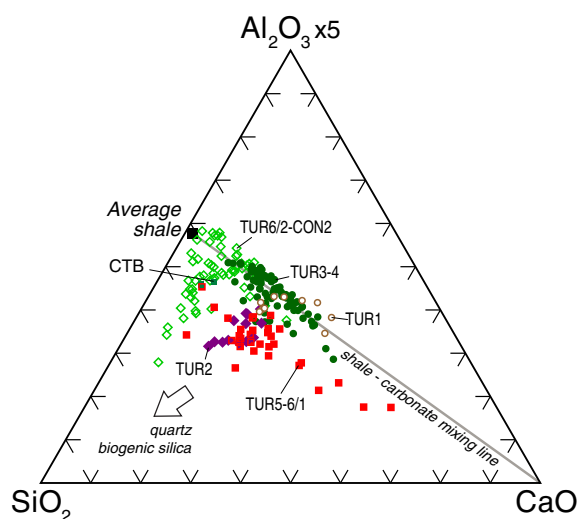

Fig. 4. Al_2O_3-SiO_2-CaO triangular plot of Bch-1 samples, illustrating the dominantly three-component system. A mixing line between carbonate and average shale (Wedepohl, 1971) predominates in finer grained strata (Sequences TUR1, TUR3–4) with scatter towards the SiO_2 apex induced in coarser grained facies (e.g. TUR2, TUR5–6) by addition of increased quartz silt and/or biogenic silica. CTB = Cenomanian–Turonian boundary samples (filled green squares).

silica (TUR6/2–CON2) contents. Carbonate concentrations vary through the Lower–Middle Turonian, but fall very significantly through the uppermost Turonian, to ~4% $CaCO_3$ at the top of the stage (Figs. 3, 4). A carbonate-rich interval (35% $CaCO_3$) characterises the base Coniacian, with lower values above (16%).

Despite their dark colour, the sediments are relatively organic lean, with total organic carbon (TOC) contents of 0.2–0.9 wt%, generally lower than an average shale value of 0.8% (Mason and Moore, 1982). The TOC profile (Fig. 3) shows little variation through the Lower and Middle Turonian, averaging 0.42 wt%. In the Upper Turonian TOC increases to around 0.65 wt% as the lithology becomes coarser grained. TOC remains high into the Lower Coniacian, showing a small gradual decrease at the top of the core. Phosphorus shows a long-term trend that is broadly comparable to Al, but displays a significantly different shorter-term cyclic variation and maxima in the low Middle Turonian and basal Coniacian.

3.2. Elemental variation and sea-level change

The Al profile and its correlatives display a strong resemblance to the long-term T/Rmax / shore-proximity curve for the SE depocentre (Fig. 3). The T-Rmax curves were constructed by Uličný et al. (2014) from proximal–distal facies correlation panels crossing the Bohemian Cretaceous Basin. Each regressive maximum was derived from the

lateral position of the regressive limit of delta-front/upper shoreface sandstones, correlated into the Bch-1 section and plotted at a corresponding depth, as a distance from Bch-1 site. In this regard, the T-Rmax curve is constructed as a 'shore proximality through time' diagram that can be applied in a manner analogous to the more commonly-used T–R curve. The derivation and limitation of these curves were discussed by Uličný et al. (2014). For Bch-1, decreasing Al (clay) and increasing Si (silt) contents in central basin hemipelagic sediments during regressions, and higher Al values with transgression, may be attributed, at least in part, to proximity-controlled grain-size effects.

Geochemical parameters considered by Jarvis et al. (2001, 2008) to be key proxies for sea-level change in hemipelagic sediments are plotted in Fig. 5. Coincident long-term peaks in Si/Al, Ti/Al and Zr/Al in the basal Middle Turonian (Sequence TUR2) and the mid-Upper Turonian (TUR6/1) provide evidence of regressive packages interpreted to consist of silt-rich sediments with higher quartz and heavy mineral contents. Outside of these packages, Si/Al ratios are relatively constant and close to that of average shale (3.0 M/M; Wedepohl, 1971), except towards the top of the core in the Lower Coniacian where diagenetic silicification occurs.

The Ti/Al profile shows particularly coherent medium- and long-term trends (Fig. 5). The regressive packages of sequences TUR2 and TUR6/1 with high Ti/Al ratios are superimposed on a long-term rising trend from 25–34 mM/M through the Lower to high Upper Turonian,
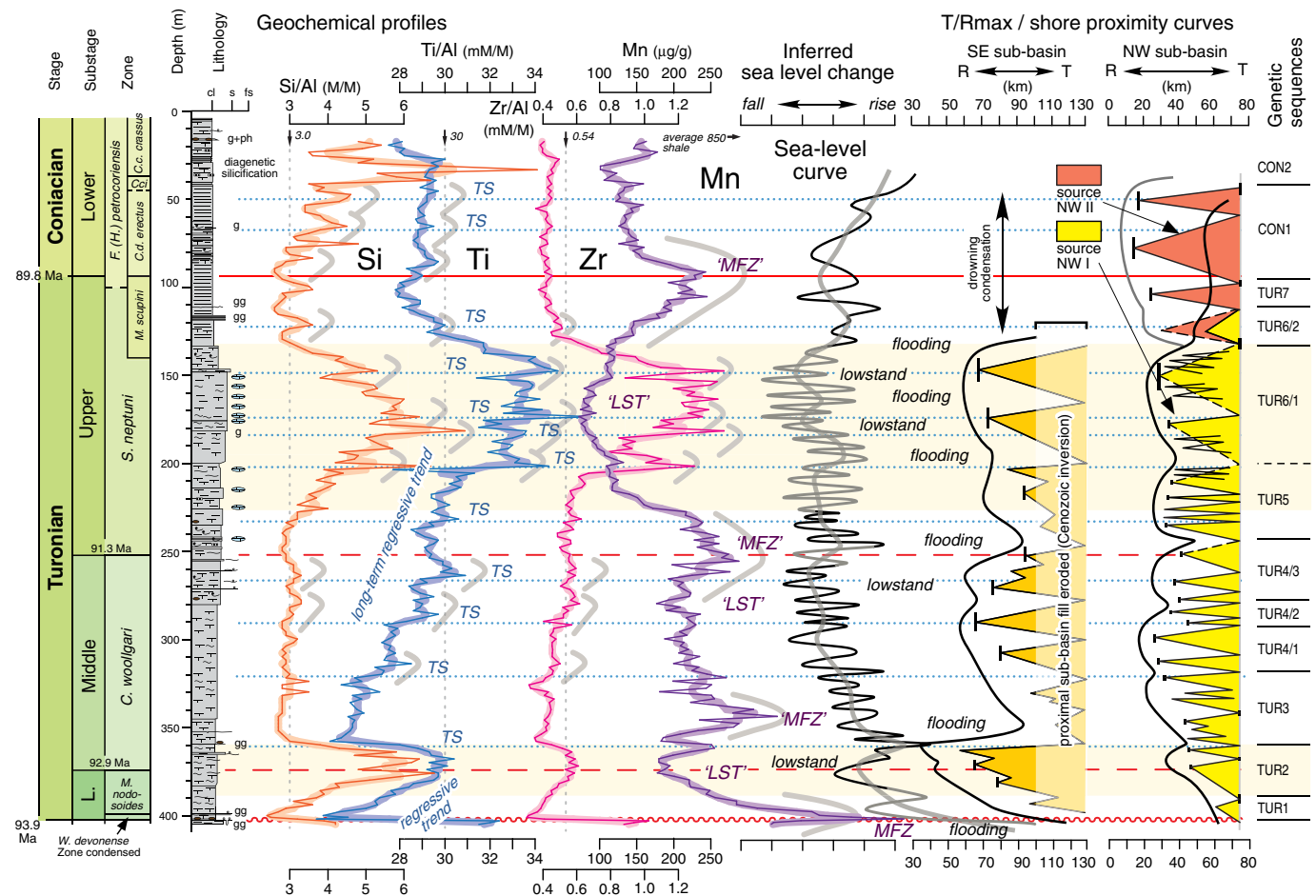

Fig. 5. Chemostratigraphic profiles of Si/Al, Ti/Al, Zr/Al and Mn for the Bch-1 core plotted against inferred sea-level change and transgressive-regressive curves from the SE and NW sub-basins and their genetic sequences. Thin solid coloured lines link all data points (2-m spacing); thicker paler lines are three-point moving averages. Thick grey curves indicate significant medium-term features for individual proxies, interpreted to represent major stratal surfaces and sequence stratigraphic intervals. Transgressive surfaces ('TS') defined from coincident peaks in Si/Al, Ti/Al and/or Zr/Al. Lowstand systems tracts ('LST'), and maximum flooding zones ('MFZ') are interpreted from the Mn profile. Key intervals displaying medium-term (0.4–1 Myr) "flooding" or "lowstand" based on the inferred sea-level changes derived from stratal geometries, are also indicated. Grey portions of the short-term inferred sea-level curve are intervals of greater uncertainty. Pale blue horizontal dotted lines aid correlation between chemostratigraphic break points and the T/Rmax curves. Pale yellow horizontal bands are major regressive packages. See Fig. 3 for key to lithology.

followed by a marked fall back to lower values below the Turonian–Coniacian boundary (28 mM/M). Values are higher and relatively stable at ~29 mM/M in the Lower Coniacian. This is interpreted to represent two long-term regressive cycles each terminated by rapid transgression.

It is notable that Zr/Al (and Zr/Ti) ratios are significantly enriched only in the Upper Turonian regressive package, where ratios rise from average shale values of 0.54 mM/M to >1.2 mM/M. This may be partly caused by the grain size increase to silty muds (Fig. 5; cf. Bertrand et al., 1996), but likely reflects also a provenance change from a dominantly SE source in the Early Turonian, to a NW or mixed NW/SE more 'granitic' provenance in the Late Turonian.

Ti/Al ratios have been shown to be a sensitive proximality and provenance indicator (e.g. Pearce and Jarvis, 1995; Chen et al., 2013). Multiple medium-term Ti/Al cycles are evident within most genetic sequences (Fig. 5). These are characterised by sharp rises of ~1 mM/M and gradual falls forming small asymmetric peaks in the Ti/Al profile. The bases of most of these cycles correlate, within error, to prominent regressive maxima in the basin, principally from the SE source region (Fig. 5). They are interpreted to represent transgressive surfaces (TS) and packages following maximum regression. Many of these TS show coincident, but less marked, enrichments in Si/Al and/or Zr/Al, as described in the English Cenomanian by Jarvis et al. (2001, 2008).

The manganese curve displays a broad similarity to the Al profile (compare Figs. 3 and 5) indicating the likely influence of the clay flux on Mn contents. However, Mn and Al are statistically uncorrelated ($R^2 = 0.06$), highlighting the complexity of Mn geochemistry, which has carbonate, clay mineral, organic matter and oxyhydroxide associations (see Jarvis et al., 2001 and Le Callonnec et al., 2014 for discussion). Long-term Mn minima, indicative of sea-level lowstands, are coincident with the regressive packages identified from the Ti/Al ratio data, with a further interval in the mid-Middle Turonian (TUR4/1–4/2). Maximum flooding zones (MFZ) are indicated by broad Mn peaks in the basal Lower Turonian (TUR1), in the low Middle Turonian (TUR3), around the Middle–Upper Turonian boundary (TUR4/3–base TUR5), and spanning the Turonian–Coniacian boundary (TUR7–CON1; Fig. 5).

A tentative eustatic sea-level curve derived from the shore proximity data in the NW and SE sub-basins, based on criteria discussed in detail by Uličný et al. (2009), is shown in Fig. 5 (after Uličný et al., 2014). Theoretically, any temporary acceleration in subsidence can cause a transgression, and therefore only those maximum transgressive surfaces that correlate between the two sub-basins are evaluated as being potentially eustatically driven and, where possible, have been verified by data from other basins. In a subsiding basin, it is the evidence for basin-scale base-level falls counteracting subsidence (i.e. not driven by temporary uplift) that can be evaluated with greater confidence as reflecting eustasy. Offlapping stratal geometries, long progradation distances, and downdip coarsening of grain size are used to interpret regressions forced by base-level falls (cf. Posamentier and Allen, 1999), and to infer extra-basinal (mainly eustatic) controls on base level.

The sea-level curve (Fig. 5) shows short-term lows where forced regressions are interpreted in the NW sub-basin, or simultaneously in both sub-basins. Estimates of magnitudes of individual sea-level cycles are necessarily speculative, in the order of 10 m in most cases. Superimposed intermediate to long-term trends (deepening / shallowing) are interpreted from successions of short-term fluctuations in which relative elevations of successive sea-level minima are based on the relative positions of maximum regressive shorelines, after intrabasinal factors such as initial palaeodepth, increased supply, or uplift are considered. A higher long-term subsidence rate through time required larger magnitudes of short-term sea-level falls to cause forced regressions.

Deep-marine sediments in the South China Sea and Japan Sea deposited since 220 ka show Ti/Al ratio trends that correlate well with eustatic sea-level change (Chen et al., 2013 and references therein): glacial lowstands and stadials are marked by high Ti/Al ratios; values have fallen by 4 mM/M with sea-level rise since the last glacial maximum

around 18 ka. Similarly at Bch-1, the Ti/Al profile exhibits 6 mM/M variation that mirrors the sea-level curve. In most cases the Ti/Al-defined transgressive surfaces and their overlying asymmetric peaks coincide with both significant short-term (100 kyr) episodes of sea-level rise and the onset of medium- to long-term (0.4–2 Myr) flooding.

The sequence stratigraphic interpretation of the long-term Mn curve (cf. Corbin et al., 2000; Jarvis et al., 2001, 2008; Renard et al., 2007) is generally consistent with the geometrically-derived eustatic sea-level curve (Fig. 5). Manganese exhibits minima coincident with major third-order sea-level lowstands, rising values accompany flooding through transgressive systems tracts, maxima occur during intervals of maximum flooding, and declining values characterise later highstands. However, the major early Middle Turonian base-TUR3 flooding event is picked out by a moderate Mn peak, but the main broad maximum, interpreted to represent a 'MFZ', occurs higher in TUR3. Manganese trends though the remainder of the Turonian generally correlate as expected with the sea level curve, although Mn shows little medium-term variation within Sequences TUR5–6/1, despite evidence of significant sea-level change. Early Coniacian flooding (mid-CON1–CON2) was accompanied by falling rather than rising Mn contents.

The Bch-1 results confirm that elemental chemostratigraphy of hemipelagic sediments offers an independent basis for interpreting medium- to long-term (0.4–2 Ma; i.e. third- to fourth-order) sea-level change, the proxies reflecting a combination of proximality and depth trends. However, short term (100 kyr) episodes of sea-level change, evident from the shore proximity curves, are generally not resolved by the elemental data.

3.3. Stable-isotope stratigraphy

A high-resolution $\delta^{13}C_{org}$ curve for bulk organic matter (which is dominantly of marine origin) from the Bch-1 core is shown in Fig. 6 (data from Uličný et al., 2014). Based on the currently assigned ages of the base Turonian at 93.89 Ma and the base Coniacian at 89.75 Ma (Fig. 6; Meyers et al., 2012; Ogg et al., 2012; Sageman et al., 2014), the 50 cm sampling interval employed here represents 5.5–5.8 kyr. This permits comparison to the highest-resolution $\delta^{13}C$ curves available elsewhere. The isotope curve is well constrained by inoceramid bivalve and ammonite datum levels recorded in the core (filled symbols) or correlated from adjacent sections (open symbols), and by calcareous nannofossil and dinocyst records (Fig. 6). Correlation to biostratigraphically calibrated carbonate carbon stable-isotope ($\delta^{13}C_{carb}$) profiles from localities in England, Spain and Germany (Uličný et al., 2014; Jarvis et al., 2015; Olde et al., 2015) has enabled the recognition of 8 major named Turonian and one Coniacian Carbon Isotope Events (CIE; Jarvis et al., 2006) in Bch-1, further enhancing stratigraphic resolution.

The major positive $\delta^{13}C$ excursion that characterises the Cenomanian–Turonian boundary interval world-wide (the CTB CIE; OAE2) was not sampled at Bch-1; the upper part of the excursion is unrepresented due to hiatuses present in the lowest few metres of the core. High $\delta^{13}C_{org}$ values ~-25.6 ‰ (VPDB) in the basal Lower Turonian *Watinoceras devonense* Zone correlate to the Holywell positive CIE (Fig. 6).

Erratic values through the Lower Turonian terminate with a minimum of −26.3 ‰ at the top of the substage, a short distance below the correlated FO of *C. woollgari* (Lulworth negative CIE). The isotope curve then rises via a series of $\delta^{13}C_{org}$ peaks to a maximum of −25.1 ‰ in lower TUR3; the penultimate peak is correlated to the Round Down positive CIE (Olde et al., 2015). A long-term decline through the Middle to basal Upper Turonian is interrupted by a short-term minimum in Sequence TUR4/2 (-26.5 ‰, Glynde negative CIE), and then a well-defined short peak (−25.7 ‰) within the upper Middle Turonian, at the base of Sequence TUR4/3, the 'Pewsey' positive CIE.

A marked long-term minimum of ~ -26.5 ‰ $\delta^{13}C_{org}$ (Bridgewick negative CIE) occurs within lower Upper Turonian Sequence TUR5,
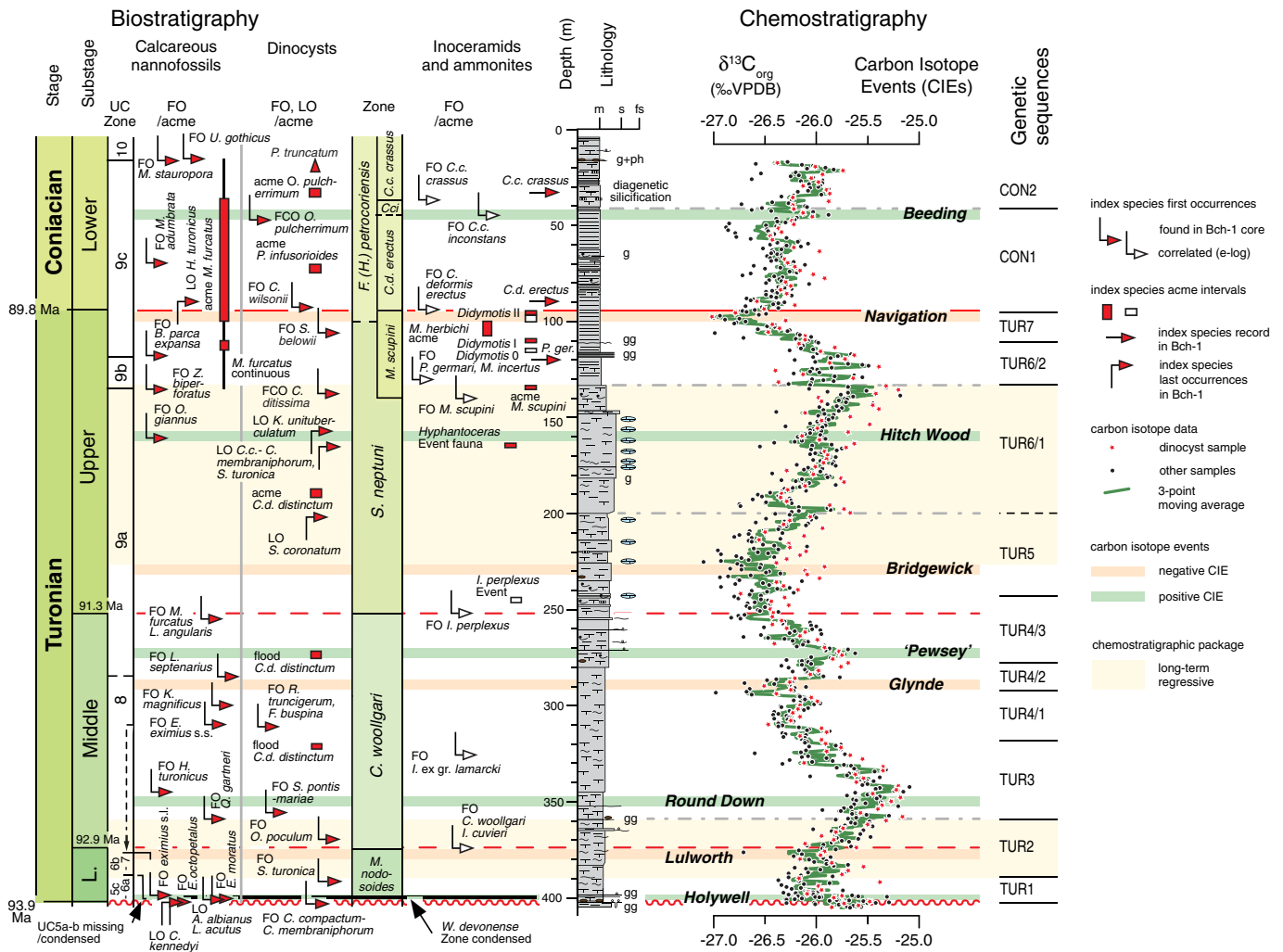
Fig. 6. Biostratigraphy and carbon-isotope chemostratigraphy of the Bch-1 well. Calcareous nannofossil, dinocyst, inoceramid bivalve and ammonite data are plotted against TOC, carbon-isotope ratios of bulk organic matter ($\delta^{13}C_{org}$), transgressive-regressive curves from the SE and NW sub-basins, and regional genetic sequences of Uličný et al. (2009). Carbon isotope events (CIEs) of Jarvis et al. (2006) are placed following Olde et al. (2015); the position of the Hitch Wood CIE is based on the Upper Turonian maximum of the $\delta^{13}C_{carb}$ curve (not presented here). Red stars are values for palynological samples, black dots are other $\delta^{13}C_{org}$ data; green line is a three-point moving average of all $\delta^{13}C_{org}$ values.

and $\delta^{13}C_{org}$ values then gradually rise, peaking in the high Upper Turonian at the top of Sequence TUR6/1. A minor $\delta^{13}C_{org}$ trough in mid-TUR6/1, a short distance above the *Hyphantoceras* macrofaunal Event (Fig. 6), is correlated to the Hitch Wood CIE (see below). A rapid fall to a second well-defined minimum of −27.0 ‰ $\delta^{13}C_{org}$ around the level of the *Didymotis* II Event, the Navigation negative CIE, occurs immediately below the correlated FO *Cremnoceramus deformis erectus* (Meek), marking the base of the Coniacian Stage. A gradual and fluctuating increase is apparent through the Coniacian part of the section, with a minor peak immediately above the correlated FO *C. crassus inconstans* (Woods), assigned to the Beeding positive CIE.

The Upper Turonian $\delta^{13}C_{org}$ maximum at Bch-1 near 135 m depth does not correspond to the maximum in correlative $\delta^{13}C_{carb}$ profiles elsewhere (Uličný et al., 2014), but seems to have a counterpart in the new composite Western Interior $\delta^{13}C_{org}$ curve (Joo and Sageman, 2014). Biostratigraphic evidence (positions of the *Hyphantoceras* Event, FO and acme *Mytiloides scupini* Heinz) indicates that a well-defined Upper Turonian long-term $\delta^{13}C_{carb}$ maximum recorded at Bch-1 (Jarvis et al., 2015) and in other European sections (Voigt and Hilbrecht, 1997; Wiese, 1999; Jarvis et al., 2006) marks the Hitch Wood positive CIE, but this falls within a continually rising $\delta^{13}C_{org}$ section at Bch-1 (Fig. 6). This temporary divergence between the $\delta^{13}C_{carb}$ and $\delta^{13}C_{org}$ profiles requires further investigation

3.4. Palynology

The 198 palynological samples processed from Bch-1 all yielded diverse dinocysts assemblages, with spores, pollen, foraminiferal test linings and acritarchs (*Veryhachium* sp.) also present. Ninety-two species and subspecies were identified (Appendix A). The ranges of selected species are plotted in Appendix B. The relative abundances of common taxa are plotted in Fig. 7 and their corresponding absolute abundances (carbonate-corrected dinocysts per gram, dpg) are shown in Fig. 8.

3.4.1. Dinocyst biostratigraphy

The dinocyst biostratigraphy of Bch-1 has been described in detail elsewhere (Olde et al., 2015). No Cenomanian dinocyst marker species were recognised in the Bch-1 core. For example, *Adnatosphaeridium tutulosum* and *Litosphaeridium siphoniphorum*, which have last occurrences in the Upper Cenomanian *M. geslinianum–N. juddii* zones (Foucher, 1981; Costa and Davey, 1992; Dodsworth, 2000; Pearce et al., 2009) are absent. However, calcareous nannofossil records place the base Turonian at 402 m (Fig. 6; Uličný et al., 2014): sediments from the bottom of the core (404.6–402.4 m) yield a Cenomanian nannofossil assemblage, including *Lithraphidites acutus* Verbeek & Manivit, *Axopodorhabdus albianus* (Black) and *Corollithion kennedyi*
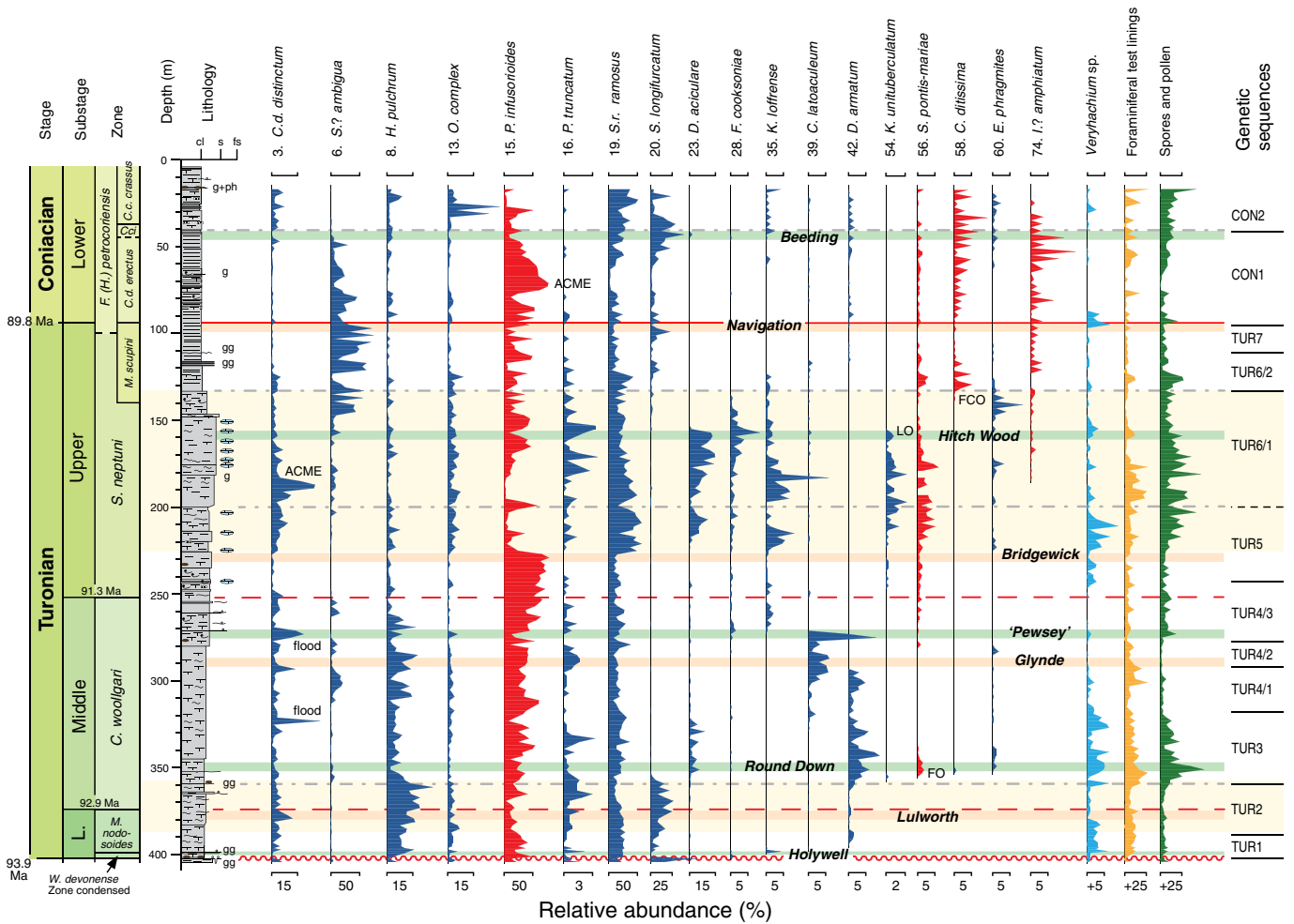
Fig. 7. Relative abundance of common dinocyst species and other palynomorphs in the Bch-1 well. Values derived from counts of 300 identified dinocysts per sample. Note the different scales used to enhance stratigraphic trends. Red fills indicate peridinioid (P-cysts) and blue fills gonyaulacoid (G-cysts) species. Assemblages are dominated by *P. infusorioides* and *S. ramosus ramosus* and, in the Turonian–Coniacian boundary interval, *S. ambigua*.

Crux. The base of the Turonian (Sequence TUR1) is placed above a burrowed omission surface at 402.35 m, overlain by a 70 cm thick zone of glauconite-rich marlstone with phosphate concretions, interpreted as a hiatus, followed by condensed deposition (Valečka and Skoček, 1991; Uličný et al., 1993; Čech et al., 2005). The first occurrence (FO) of the Lower Turonian UC5c species *Eprolithus octopetalus* Varol at 401.2 m and the UC6b index species *Eprolithus moratus* (Stover) at 401.0 m depth indicates that at least nannofossil zones UC 5c–6a are contained in the lowermost 1.35 m of the Turonian succession in Bch-1.

A succession of 18 dinocyst datum levels, considered to be of potential regional biostratigraphic significance, are recognised in Bch-1 (Fig. 6). From bottom to top, these are: (a) FOs of *Cyclonephelium compactum-Cauveridinium membraniphorum* 'group' and then *S. turonica* in the Lower Turonian; (b) FOs of *O. poculum*, *S. pontis-mariae*, a flood of *C. distinctum distinctum*, the FOs of *R. truncigerum* and *F. buspina*, and a second flood of *C. d. distinctum* in the Middle Turonian; (c) last occurrence (LO) of *S. coronatum*, a *C. d. distinctum* acme, the LOs of *C. compactum-C. membraniphorum* 'group', *S. turonica* and *K. unituberculatum*, the first common occurrence (FCO) of *C. ditissima* and FO of *S. belowii* in the Upper Turonian; (d) FO of *C. wilsonii* coincides with the base Coniacian, followed by an acme of *P. infusorioides*, the FCO and then an acme of *O. pulcherrimum*. *Pervosphaeridium trunctatum* ranges to the top of the sampled section (high Lower Coniacian).

With the exceptions of *K. unituberculatum*, *S. pontis-mariae* and *C. ditissima*, most of these taxa occur sporadically (Appendix B) and in low numbers (<1% of assemblage), limiting stratigraphic resolution.

However, comparison with dinocyst records from the Cenomanian–Coniacian of southern England and northern France demonstrates the stratigraphic utility of the above records, and has enabled the development of a revised northern European Turonian dinocyst zonation scheme (Olde et al., 2015).

3.4.2. Dinocyst assemblage trends

Samples yielded on average 21 dinocyst species, with *Spiniferites ramosus ramosus* and the peridinioid cyst *Palaeohystrichophora infusorioides* constituting the main components in assemblages through most of the section. This 'Spiniferites-Palaeohystrichophora Assemblage' (S-P) coined by Prince et al. (1999), dominated by the peridinioid cyst, is characteristic of Late Cretaceous offshore/deeper water environments and upwelling zones (Prince et al., 1999, 2008; Pearce, 2000). It contrasts to low-diversity assemblages dominated by gonyaulacoid cysts, particularly *Circulodinium*, *Heterosphaeridium* and *Senoniasphaera*, originally referred to as the *Senoniasphaera–Heterosphaeridium* assemblage by Prince et al. (1999). Pearce (2000) and Pearce et al. (2003) considered the 'Circulodinium–Heterosphaeridium Assemblage' (C-H) to be a more suitable name due to the sporadic occurrence of *Senoniasphaera*, and found the assemblage to characterise near-shore/shallow-water environments, and typically lack peridinioid and opportunistic cosmopolitan species.

A number of distinctive dinocysts range patterns are observed in the Bch-1 data (Figs. 7, 8). A generally inverse relationship between the relative abundance curves of *P. infusorioides* and *S. r. ramosus*, with a marked minimum of the former and an acme of the latter in Upper
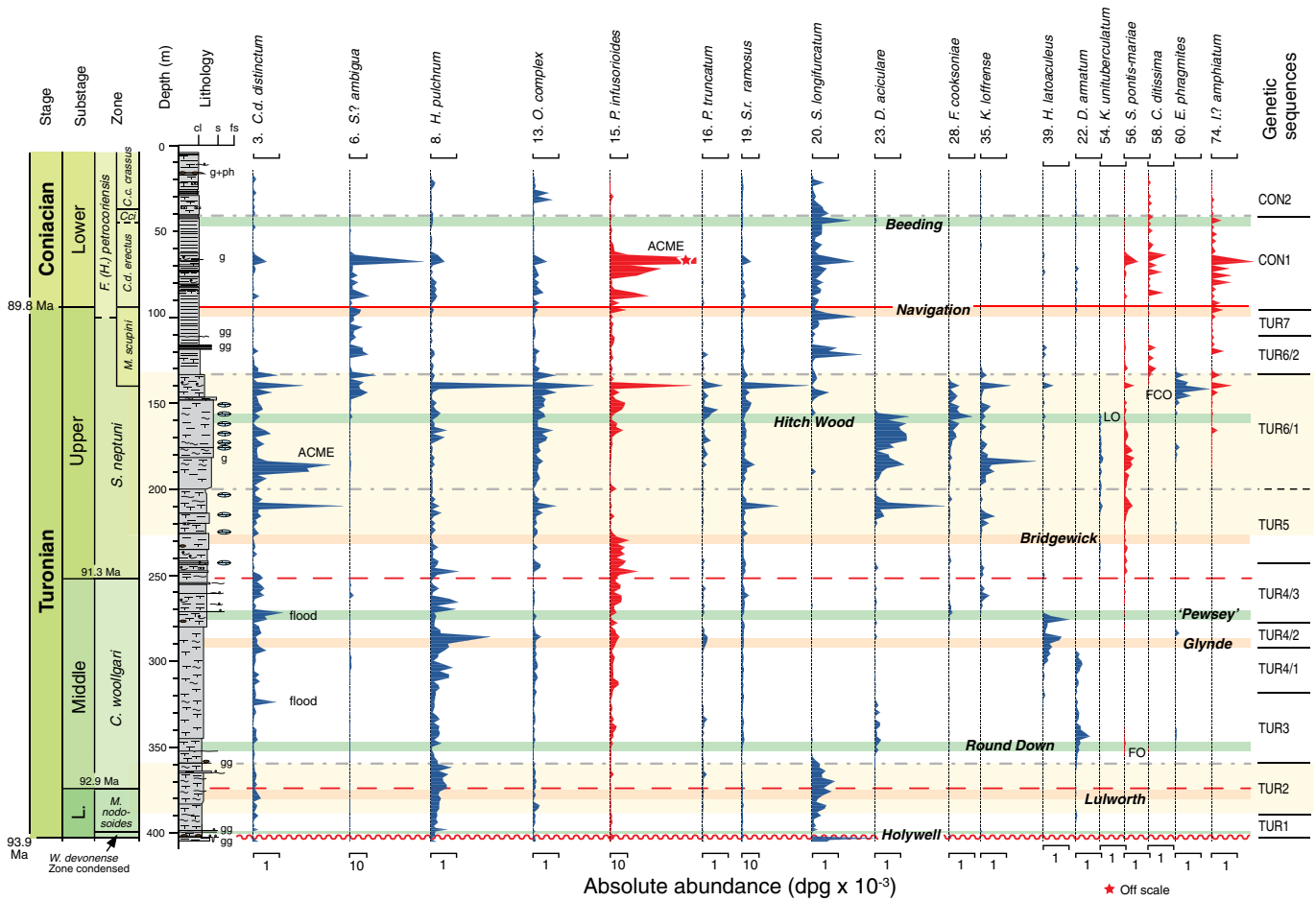
Fig. 8. Absolute abundance of common dinocyst species in the Bch-1 well. Absolute abundances are dinocysts per gram (dpg) in the non-carbonate fraction of the sediment (see text for detail). Red fills indicate peridinioid (P-cysts) and blue fills gonyaulacoid (G-cysts) species.

Turonian Sequences TUR5–6/2 (Fig. 7), reflects the numerical dominance of these two taxa in the assemblages. Absolute abundances of individual species vary widely on a sample-to-sample basis (Fig. 8). Marked dinocysts abundance peaks at 67.5 m, 139.5 m and 209.5 m contain diverse assemblages; the first of these coincides with a very pronounced Lower Coniacian acme of *P. infusoriodes*. A well-defined acme of *C. d. distinctum* occurs 185–190 m in mid-Upper Turonian Sequence TUR6/1, with lesser floods of the species below, in the Middle Turonian at 323.5 m (TUR3) and 271.5 m (TUR4/3).

Lower Turonian to basal Middle Turonian assemblages (Sequences TUR1–2) include relatively high proportions of *Hystrichosphaeridium pulchrum* and *Surculosphaeridium? longifurcatum* (Fig. 7). *Downiesphaeridium armatum* is most common in Middle Turonian Sequences TUR3–4/1, coincident with increased numbers of spores, pollen and acritarchs, and an acme of *Circulodinium latoaculeum* occurs in TUR4/3. Other notable events (Appendix B) include the LO *Microdinium distinctum* and last common occurrences (LCOs) of *Hystrichospheridium bowerbankii* and *Achomosphaera sagena* towards the top of the Middle Turonian (Sequence TUR4/3).

In addition to terrestrial palynomorphs (spores and pollen), a number of dinocysts species are more common and more abundant within the regressive Upper Turonian package of Sequences TUR5–6/2, notably *Downiesphaeridium aciculare*, *Oligosphaeridium prolixispinosum*, *Florentinia cooksoniae*, *Hystrichosphaeridium tubiferum brevispinum*, *Kleithriasphaeridium loffrense*, *Kiokansium unituberculatum*, *S. pontismariae*, *Tanyosphaeridium salpinx* (Figs. 7–8, Appendix B). Common species that temporarily disappear within this interval are *Florentinia mantellii* and *Downiesphaeridium armatum*. The mutual exclusivity of a number of key taxa, points to palaeoenvironmental factors limiting their stratigraphic distribution in the Bohemian Cretaceous Basin.

A number of well-defined FOs of common species is apparent in the section (Appendix B), notably, *Florentinia clavigera* towards the top of the Middle Turonian, and *Isabelidinium amphiatum* in the mid-Upper Turonian. *Surculosphaeridium belowii* and *Cribroperidinium wilsonii* first occur within the Turonian–Coniacian boundary interval, which from the summit of Sequence TUR6/1 to mid-Sequence CON1, is characterised by assemblages containing abundant *Sepispinula? ambigua*.

3.4.3. Species richness and abundance

Species richness (number of species and subspecies identified per sample) and palynomorph abundance data are plotted in Fig. 9. Species richness averages 22 in the uppermost Cenomanian–Lower Turonian and a diversity minimum occurs in the basal Middle Turonian, immediately above the Lulworth CIE. However, values increase rapidly within the lower Middle Turonian to a well-defined maximum of 38 in the lower part of Sequence TUR3 (Fig. 9) coincident with the Round Down CIE. There is no increase in dinocyst abundance at the Middle Turonian species richness maximum. The peak in species richness is generated by a 10 m thick interval that exhibits multiple FOs (Appendix B): *Hystrichosphaeridium conospiniferum*; *H. salpingophorum*; *Stephodinium coronatum*; *Hystrichostrogylon membraniphorum*; *Odontochitina singhii*; *Kiokansium unituberculatum*; *Nematosphaeropsis densiradiata*; *Subtilisphaera pontis-mariae*; *Wrevittia* cf. *cassidata*; *Chatangiella ditissima*; *Cometodinium whitei*; *Exochosphaeridium phragmites*; *Tanyosphaeridium variecalamus*; and *Sentusidinium* sp. B.
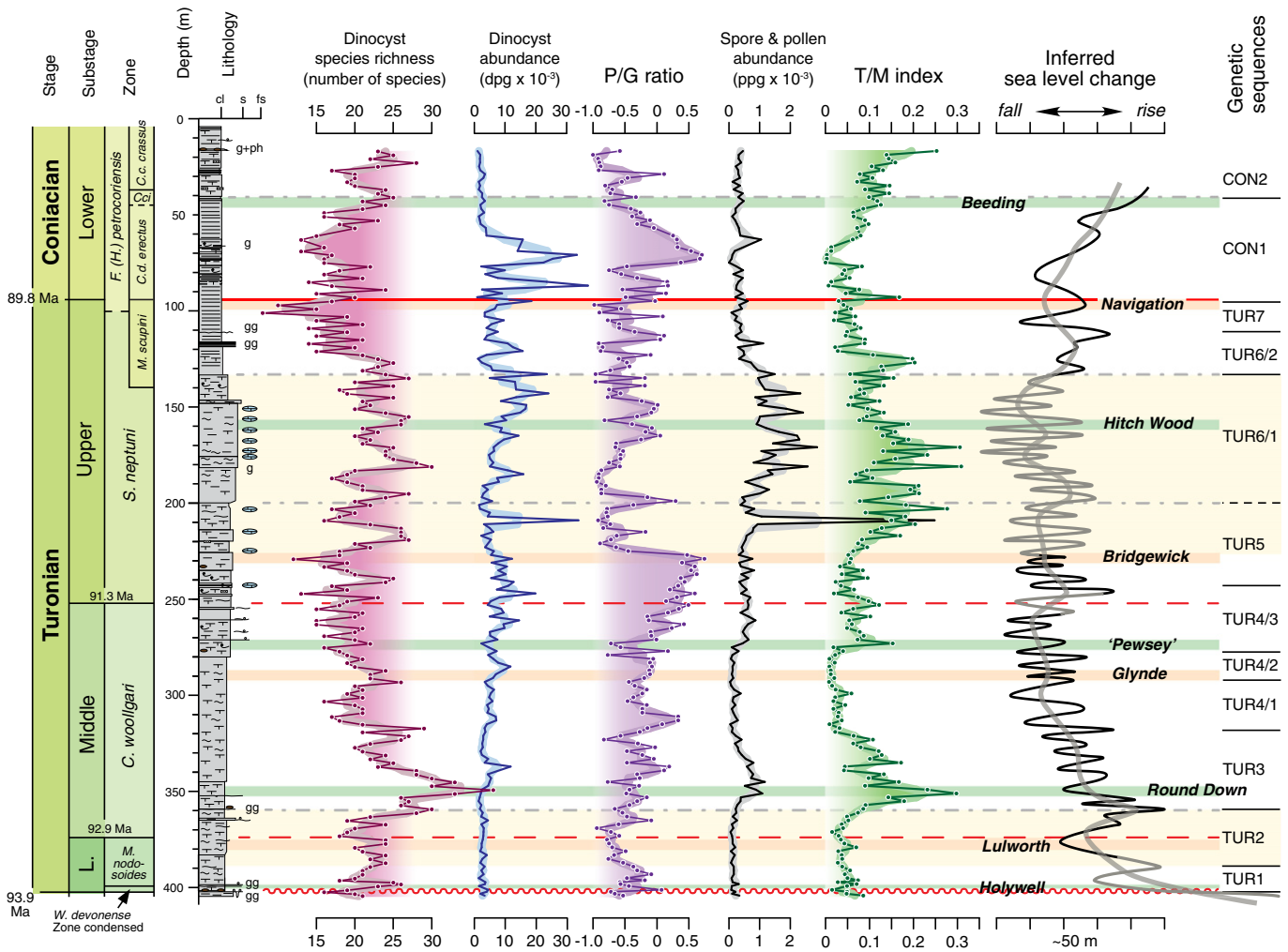
Fig. 9. Dinocyst (species richness, abundance, P/G ratio) and terrestrial palynomorph (spore and pollen abundance, T/M index) variation in the Bch-1 well compared to the sea-level curve of Uličný et al. (2014). Dinocyst species richness is the total number of dinocyst species and subspecies identified in each sample. Dinocyst and other palynomorph abundances are reported per gram of the non-carbonate fraction of the sediment (dpg, ppg). The P/G ratio is the ratio between the number specimens of P- and G-cysts counted (within the total count of 300 dinocysts); see text for explanation of P- and G- cyst types. T/M index is ratio of terrestrial palynomorphs (spores and pollen) to terrestrial plus marine palynomorphs (dinocysts, acritarchs, foraminiferal linings).

Dinocyst species richness declines (but remains on average 22) through the Middle Turonian, reaching a minimum of 12 in the basal Upper Turonian at 230 m, coincident with the Bridgewick CIE. The CIE also represents a break point on the dinocyst abundance curves with rising values from <750 dpg to >5000 dpg through the Lower and Middle Turonian being driven by increasing P-cyst (*P. infusorioides*) abundances that crash at this level. This is illustrated by the rise then massive fall in the P/G ratio immediately above the Bridgewick CIE (Fig. 9).

High and cyclically fluctuating species richness (16–30) characterises the regressive package of the Upper Turonian (Sequences TUR5–6). This high diversity is caused by the addition of species to the persisting assemblage, some of which are the same as those that caused the diversity peak in TUR3 (*K. unituberculatum, S. pontis-mariae, C. d. distinctum, E. phragmites*). Here, and elsewhere, species richness commonly peaks during periods of sea-level rise (Fig. 9), but shows no consistent correlation to dinocyst abundance or terrestrial palynomorph trends. Dinocyst abundances fluctuate considerably through the Upper Turonian (2000–34,000 dpg), but in contrast to the Lower and Middle Turonian, abundance is here driven predominantly by G-cyst rather than P-cyst variation (Figs. 7–9).

A well-defined long-term minimum of 8–10 species occurs at the top of the Turonian, coincident with the Navigation CIE. Values rise

through the Lower Coniacian, with a medium-term peak at the Beeding CIE, and up to 28 species occur towards the top of the core. Dinocyst abundance shows peaks of >30,000 dpg in the lowest Coniacian *C. d. erectus* Zone due to an acme of *P. infusorioides* (Fig. 7), but falls back to lower levels above, along with an increasing diversity.

3.4.4. P/G ratio

Species richness and dinocyst abundance curves show no correlation (Fig. 9), but the latter displays a similar trend to the P/G ratio, which itself closely follows the relative abundance profile of *P. infusorioides* (Fig. 7). This demonstrates that both P/G ratio and overall dinocyst absolute abundance are controlled largely by variation in *P. infusorioides* content.

The P/G ratio is moderate and generally falling through the Lower Turonian to a minimum approaching − 1.0 in the basal Middle Turonian (corresponding to <100 dpg of *P. infusorioides*), but then increases dramatically through the Middle Turonian into the basal Upper Turonian (Sequences TUR3–5; Fig. 9). Values rise to a maximum of + 0.7 (associated with 10,000 dpg of *P. infusorioides*) in the middle of basal Upper Turonian Sequence TUR5 around 230 m, before falling sharply back to − 0.9 in the upper part of the sequence. The sharp drop in P/G ratio occurs immediately above the Bridgewick CIE (Fig. 9). This corresponds to the base of the Upper Turonian regressive
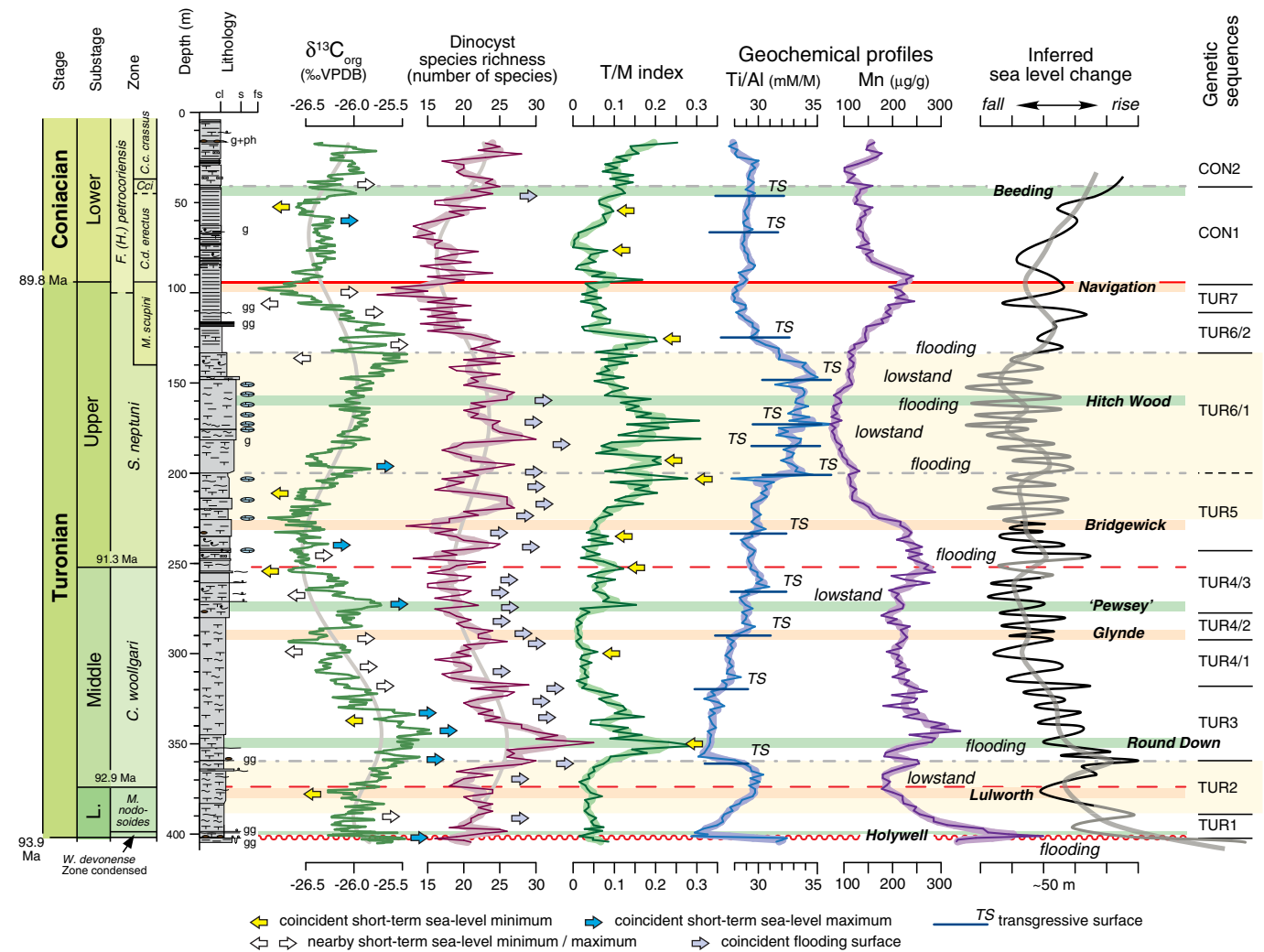
Fig. 10. Comparison between sea-level proxy records in Bch-1 and the sedimentologically derived sea-level curve for the Bohemian Cretaceous Basin. Grey curves on the $\delta^{13}C_{org}$ and dinocyst species richness profiles are 7th-order polynomial fits; the similarity between the long-term trends of the two parameters is striking.

package revealed by the chemostratigraphic data (Figs. 3, 5). P/G ratios show no correlation with species richness or T/M index in the Lower and Middle Turonian.

Low P/G ratios (<−0.8) through the mid-Upper Turonian, upper part of Sequence TUR5 and Sequence TUR6/1, are punctuated by a peak of +0.3 at the sequence boundary (Fig. 9). P/G ratios rise through the lower part of Sequence TUR6/1 to a value of +0.1 at 165.5 m below the Hitch Wood CIE. Values fluctuate erratically between −1.0 and +0.1 through the remaining Upper Turonian–basal Coniacian interval, where variations in G-cysts abundance are significant. Low P/G ratios accompany the Navigation CIE, but rise sharply above. The acme of *P. infusorioides* around 72 m (Figs. 7, 8) drives P/G ratios back to a long-term peak of +0.7 in the basal Lower Coniacian (*C. d. erectus* Zone), before declining back to −1.0 at the top of the core. Intervals with high P/G ratios generally correspond to intervals having low T/M index values and vice versa, although there is no correlation on a sample-by-sample basis.

3.4.5. Terrestrial palynomorph abundance and the T/M index

The T/M index profile broadly follows the spore and pollen abundance curve (Fig. 9), demonstrating that it is the terrestrial palynomorph flux rather than varying dinocyst input that largely controls T/M variation. Major features are: (1) broad abundance and

T/M index peaks in Middle Turonian Sequence TUR3, with maxima of 700 ppg and T/M ~ 0.3 near the base, coincident with the Round Down CIE; (2) step increase in the upper Middle Turonian, lower Sequence TUR4/3, at the 'Pewsey' CIE; (3) rising T/M ratios from the low Upper Turonian Bridgewick CIE, mid-Sequence TUR5, to the base of Sequence 6/1; (4) high values and multiple abundance and T/M index peaks (>1000 ppg; T/M > 0.2) through Upper Turonian Sequences TUR6/1–6/2; (5) falling values across the Turonian–Coniacian boundary with minima (<100 ppg; T/M <0.01) in the *C.d. erectus* Zone, before rising T/M ratios above, in this case unmatched by increasing abundance. The T/M index minimum in the Lower Coniacian occurs at the P/G ratio maximum and dinocyst abundance peak, driven by the very high abundance of *P. infusorioides* at this level.

Only a weak correlation exists between the T/M index plot and the inferred sea-level curve (Fig. 9). The interval of low sea levels in the Upper Turonian is, as expected, characterised by increased T/M ratios, and within this interval, peaks in T/M index commonly correspond to intervals of medium-term sea-level fall. However, the Lower Turonian regressive package of TUR2 shows no increase in the T/M index. Rather, a major peak occurs higher, in Sequence TUR3, above a sea-level maximum at the TUR2 / TUR3 boundary and within an interval of relatively high, if falling, sea levels. Additionally, in the Lower Coniacian, rising sea levels are marked by rising, not falling, T/M ratios.

4. Palaeoenvironmental analysis

4.1. Palaeoenvironmental proxies and sea-level change

T/M index (or terrestrial palynomorph abundance) and dinocyst species richness are the two palynological parameters that have been commonly proposed as sea-level proxies (e.g. Prauss, 1993, 1996, 2001; Stover et al., 1996). These are plotted in Fig. 10 against other palaeoenvironmental proxies, and the tentative sea-level curve derived from the T/Rmax shore proximity curves and other sedimentological data (Uličný et al., 2014). Following an earliest Turonian sea-level highstand, long-term sea level generally fell through the Early and Middle Turonian. Medium-term flooding events during the early Middle Turonian and early Late Turonian, were preceded by late Early Turonian and late Middle Turonian lowstands. A long-term lowstand with multiple medium- and short-term transgressions and regressions characterised most of the Late Turonian, but with a major flooding event during the latest Turonian *M. scupini* Zone. Turonian–Coniacian boundary times were characterised by a short-term flooding event superimposed on a medium term sea-level lowstand. This was followed by more consistently rising sea levels through the Early Coniacian.

Elemental geochemical sea-level proxies (Ti/Al, Mn) are generally consistent with trends in the long- (~2 Ma) and medium-term (0.4–1 Ma) sea-level curves, but do not capture short-term (~100 kyr) variation (Fig. 10). The basal Middle Turonian and Upper Turonian lowstand intervals are well displayed by maxima and minima, respectively, in the long-term Ti/Al and Mn profiles. At a finer scale, Ti/Al ratio peaks above interpreted transgressive surfaces correspond in most cases to inflection points on the medium term sea-level curve, for example, the base TUR6/1 sea-level rise and that below the Hitch Wood CIE in the same sequence. However, the low Middle Turonian Mn maximum, considered to represent major flooding, is located above the Round Down CIE, higher than the proposed medium-term peak sea level of Uličný et al. (2014). Rising sea levels through the Early Coniacian are also not matched by significant changes in Ti/Al or Mn; these proxies indicate maximum flooding coincident with the stage boundary interval (Fig. 5) and the associated drowning of the SE Bohemian Massif siliciclastic source area.

As expected, the major Upper Turonian lowstand interval (Sequences TUR5–6/1) displays elevated T/M index values with two maxima corresponding to medium-term sea level falls. Some short-term T/M maxima correspond to short-term sea-level lows (arrowed, Fig. 10) but there is no consistent relationship. It should be noted, however, that short-term sea-level cycles are relative poorly constrained in this part of the succession (denoted by grey rather than black curve in Fig. 10), and the 2-m sample spacing adopted for the palynological study is insufficient to fully capture the high-frequency cyclicity. High T/M ratios in the basal Middle Turonian correspond to the Round Down CIE short-term lowstand; those in the uppermost Middle Turonian, above the 'Pewsey' CIE, correspond to a medium-term lowstand, and a peak in the lower *M. scupini* Zone correlates to the mid-TUR6/2 short-term lowstand. It is evident that the broad Middle Turonian long-term T/M peak lies above, rather than within, the main regressive package of Sequence TUR2.

The dinocyst species richness profile displays systematic long- and short-term trends that are remarkably similar to both the $\delta^{13}C_{org}$, and the sea-level curves. In the case of the former, the baseline trend, expressed by a 7th-order polynomial fit to the data (Fig. 10), which has a cycle duration close to the 2.4 Myr long-eccentricity cycle (Uličný et al., 2014), closely matches that of the species richness data. Both have lower Middle Turonian (~Round Down CIE) and Upper Turonian (~Hitch Wood CIE) maxima, and uppermost Middle Turonian–basal Upper Turonian and Turonian–Coniacian boundary minima (~Bridgewick and Navigation CIEs). Peaks and troughs in the dinocysts species richness curve are consistently offset 10–20 m below those for the carbon isotope, although this may be due in part to the very different sampling resolution of the two data sets.

There is, however, no consistent correlation in short- to medium-term variation.

Comparison of the $\delta^{13}C_{org}$ vs. sea-level curves, analysed in detail by Uličný et al. (2014), demonstrates that despite some individual matches (arrows in Fig. 10), neither a systematic in-phase, nor out-of-phase correlation with interpreted sea-level cycles can be demonstrated. The long-term 'background' (2.4 Myr) and shorter-term (1 Myr scale) highs and lows in $\delta^{13}C$ appear to broadly correspond to intervals characterized by more pronounced short-term sea-level highs and lows, respectively, consistent with the hypothesis of rising eustatic sea level driving increased global organic carbon burial (cf. Jarvis et al., 2002). However, on the scale of intermediate (0.4–1 Myr) to short-term (100 kyr) $\delta^{13}C$ fluctuations, no systematic relationship between $\delta^{13}C$ and sea-level change is observed.

By contrast, comparison between short-term dinocyst species richness and sea-level variation demonstrates a large number of positive correlations between increases in dinocyst diversity and flooding events (pale grey filled arrows, Fig. 10). It must be emphasized that not every interpreted sea-level rise and maximum has a corresponding species richness peak, and species richness minima are less exactly matched to sea-level minima. Nonetheless, with the sole exception of the maximum at the Round Down CIE, all 8 major diversity peaks, and most minor peaks, in the Middle–Upper Turonian correspond to highstands: 14 out of 18 well-defined short-term sea-level cycles in the Middle–Upper Turonian (black line on the relative sea-level curve in Fig. 10) are clearly expressed by peaks and troughs in the dinocyst species richness record (highlighted by pale grey filled arrows). The relationship is less clear in the Turonian–Coniacian boundary interval where, despite very similar trends in the species richness and sea-level curves, peaks and troughs appear to show significant positional offsets.

4.2. Multi-proxy records of sea-level change in the Bohemian Cretaceous Basin

4.2.1. Lower and Middle Turonian

The relatively condensed nature of the Lower Turonian section at Bch-1 hinders interpretation of a detailed sea-level history. The Early Turonian was characterized by the progradation of siliciclastics into the basin from all source areas, but particularly in the SE sub-basin (Fig. 2). Importantly, the tidal circulation was dominated by flows to the NW (Mitchell et al., 2010). Sea-level proxies are consistent with generally falling eustatic sea levels towards a minimum at the summit of the substage, coincident with the Lulworth CIE (Figs. 5, 10).

The Middle Turonian shows a consistent pattern of proxy trends, with a long-term sea-level fall, marked by multiple cycles of increasing siliciclastic progradation (Fig. 10). This followed significant early Middle Turonian flooding (base Sequence TUR3), coincident with a major transgression in the SE sub-basin (Fig. 5). Dinocyst species richness, Mn and $\delta^{13}C$ rise towards, and the Ti/Al ratio reaches a plateau, during the main flooding interval at 360 m.

The T/Rmax/shore proximity curves indicate that rapid flooding was followed by a sharp and then long-term relative sea-level fall from the TUR3 sequence base (Figs. 5, 10). A step down in the Ti/Al profile at this point is consistent with flooding driving a major provenance shift, cutting off siliciclastic supply from the SE source area. However, increasing dinocyst species richness, Mn and $\delta^{13}C$, proxies for continuing sea-level rise, form prominent maxima higher in the succession, around the Round Down CIE, albeit with offset peak positions (~100 kyr).

T/M index values rise to a sharp peak coincident with a minor short-term regression following the base Sequence TUR3 flooding, but contrary to expectation, show a medium-term falling trend through the remainder of the Sequence, accompanying medium- to long-term relative sea-level fall. The T/M peak is driven principally by increased spore and pollen abundance (Figs. 7, 9), so it is not an artefact of the dinocyst record.

Uličný et al. (2014) argued that due to good water-mass circulation, marine palynomorphs dominated palynological assemblages until the end of TUR 2 deposition. The sharp increase in terrestrial palynomorphs above the base of TUR 3 is correlated to a relative sea-level fall in the early part of deposition of TUR 3, combined with uplift in the western part of the basin (Uličný et al., 2009). This event led to closure, or significant narrowing, of the NW communication of the Bohemian Cretaceous seaway with NW Europe via the 'Elbe Strait' gateway (Fig. 2), which temporarily changed the circulation pattern to that of a semi-enclosed embayment. Continued progradation of lowstand deltas from the NW is recorded in the interval of elevated T/M index values above 350 m depth; this ratio gradually decreases towards the base of TUR 4 at 318 m.

The persisting dinocyst assemblage in the Lower Turonian of Bch-1 includes forms that have been previously assigned mid-outer shelf, normal marine salinity affinities, such as *Achomosphaera*, *Spiniferites ramosus ramosus*, *Surculosphaeridium longifurcatum* and *Hystrichodinium pulchrum* (May, 1980; Harker et al., 1990; Pearce, 2000; Harris and Tocher, 2003; Pearce et al., 2003). The dinocyst diversity peak observed in lower Middle Turonian Sequence TUR3 is driven by the addition of new species to this assemblage. There is also an increase in the acritarch *Veryhachium* (Fig. 7). Some studies have shown that acanthomorph acritarchs are associated with inshore, restricted basinal environments (Wall, 1965). This interval contains high quantities of terrestrial palynomorphs, and the calcareous nannofossil *Braarudosphaera* is also observed (Fig. 11). In modern environments braarudosphaerids are found in low-salinity, near-shore waters (Bukry, 1974), and in the Turonian of Bohemia *Braarudosphaera*-rich sediments have been linked to increased terrigenous input (Švábenická, 1999). The affinity of *Braarudosphaera* for more proximal sediments has been attributed to a preference for low salinity and eutrophic conditions (Cunha and Shimabukuro, 1997; Konno et al., 2007). In some Paleocene and modern studies, a cool-water preference has also been postulated (Siesser et al., 1992; Peleo-Alampay et al., 1999).

Species of many of the additional genera appearing in TUR3 have been previously interpreted to: (1) represent some degree of reduced salinity, such as *Circulodinium*, *Cribroperidinium*, *Dinogymnium*, *Odontochitina* and *Subtilisphaera* spp. (May, 1977, 1980; Batten, 1982; Brinkhuis and Zachariasse, 1988; Lister and Batten, 1988; Harker et al., 1990; Wilpshaar and Leereveld, 1994; Leereveld, 1995; Schiøler et al., 1997); or (2) have littoral affinities, such as *Circulodinium* spp. and *Sentusidinium* spp. (Batten, 1982; Tocher, 1984; Hunt, 1987; Lister and Batten, 1988; Marshall and Batten, 1988; Wilpshaar and Leereveld, 1994; Leereveld, 1995); or (3) characterise inner to middle neritic environments, such as *Cribroperidinium* (Hunt, 1987; Lister and Batten, 1988; Marshall and Batten, 1988; Zevenboom et al., 1994; Leereveld, 1995; Pearce, 2000; Pearce et al., 2003) and *Circulodinium d. distinctum*, *Coronifera oceanica*, *Cauveridinium membraniphorum*, *Dinogymnium acuminatum*, *Downiesphaeridium*, *Ellipsodinium rugulosum*, *Hystrichodinium pulchrum*, *Impletosphaeridium clavulum*, *Microdinium*, *Senoniasphaera*, *Sentusidinium*, *Surculosphaeridium* and *Xenascus* (Pearce, 2000; Pearce et al., 2003; Figs. 7, 11).

Simplistically, the addition of 'low-salinity' or inner neritic dinocysts, terrestrial palynomorphs, acritarchs and *Braarudosphaera* implies greater shallow-water influences, and might be considered to be indicative of relative sea-level fall; inshore–offshore trends characteristically show increasing dinocyst diversity due to the addition of offshore stenotopic species to an existing inshore euryhaline assemblage. However, the continuing prevalence of outer-shelf/oceanic and normal-marine salinity-indicating taxa, point to limited sea-level change, and other proxies such as Mn indicate medium-term flooding.

The influence of efficient hypopycnal flows, along with redeposition of coarse siliciclastics in shallow water, was invoked by Uličný (2001) to explain the marked grain-size partitioning between the sand-dominated delta foresets and mud-dominated distal bottomsets and offshore regions. The addition of shallower-water dinocyst species,

proximal-indicating terrestrial palynomorphs and *Braarudosphaera* in Sequence TUR3 (Figs. 7, 11), could be due to hypopycnal flows carrying low-density fines from shallow areas to more distal parts of the basin. Hydraulic sorting during transport, with the early deposition of coarser and denser siliciclastic grains, may explain the absence of sedimentological or elemental proximity indicators coincident with the T/M index peak.

During the long-term relative sea-level highstand of the Turonian, the basin acted as a tidal-influenced seaway separating the central European Island from the Sudetic Islands (Fig. 2), facilitating water-mass exchange between the Boreal and Tethyan realms (Klein et al., 1979; Uličný et al., 2009; Mitchell et al., 2010). Tidal current action was amplified due to the funnelling effects of the passage between the Saxonian and Bohemian parts of the basin that became further narrowed by the progradation of deltas from both sides of the strait. Closure or restriction of the 'Elbe Strait' gateway accompanying the TUR3 regression (Figs. 2, 3; see above) would have had a profound effect on basin circulation; NE- and S-directed palaeocurrents determined from available outcrop data suggest that a different circulation pattern was established during TUR3 deposition compared to that in the other sequences. During the remainder of the Middle Turonian–Early Coniacian, the dominant palaeocurrent, also of tidal origin, was primarily towards the SE, along the basin axis, locally deflected by shoreline physiography (Uličný, 2001).

Through the remainder of the Middle Turonian (TUR4), species richness decreases while the abundance of P-cysts increases, peaking in the lower Upper Turonian. In modern ecosystems high productivity is commonly linked to the dominance of few species that can utilise the available nutrients by growing quickly and out-compete other species that can better prosper in specialised niches in more stable, but oligotrophic, environments, leaving a low-diversity assemblage. As terrestrial palynomorphs, *Braarudosphaera* and low-salinity dinocysts all decline through the Middle Turonian (Figs. 7, 11), it is likely that hypopycnal flows no longer influenced the assemblage, so nutrients were probably sourced by upwelling rather than by terrestrial run-off (see below, Section 4.2.5 for discussion).

4.2.2. Upper Turonian

Major palaeoenvironmental change occurred in mid-TUR5, coincident with the Bridgewick CIE (Figs. 9–11). The abundance of peridinioid cysts decreases sharply, indicating a cessation of upwelling-derived nutrients as proximal waters influenced the water mass of the depositional area. Dinocyst species richness began to generally increase again after a long decline through TUR4 and a minimum in early TUR5, and through TUR6/1 there is a number of pulses of increased diversity coincident with transgressions. These increases are related to a second influx of low-salinity or inner neritic associated dinocysts, including *C. d. distinctum*, *P. truncatum*, and *D. aciculare* (Fig. 11). Again, the dinocyst assemblage features a mix of mid-outer shelf taxa such as *Spiniferites ramosus* and *Florentinia,* alongside the 'low-salinity' forms. This interval also incorporates a re-appearance of the proximal-indicating nannofossil *Braarudosphaera,* and the acritarch *Veryhachium*, as well as increased terrestrial palynomorph abundance, increases in Si/Al, Ti/Al and Zr/Al ratios, and a long-term minimum in Mn concentration.

In contrast to the low Middle Turonian, increased grain size, high T/M indexes and Ti/Al ratios, and low Mn contents are all consistent with the medium-term sea-level lowstand indicated by T/Rmax / shore proximity data, with increased input of silt and shallower water dinocysts. Hypopycnal flows likely again became more important as a means of transporting coarser muds into the basin centre but here, unlike the Middle Turonian, there is no separation of terrestrial palynomorphs from their associated siliciclastic component. Generally shallow-water conditions and frequent T–R cycles within Sequence TUR6/1 likely contributed to both fast regressions and strong turbulent mixing, although sea-level changes need not have been of large amplitude. Again, mixing of dinocyst assemblages occurred, rather than a change
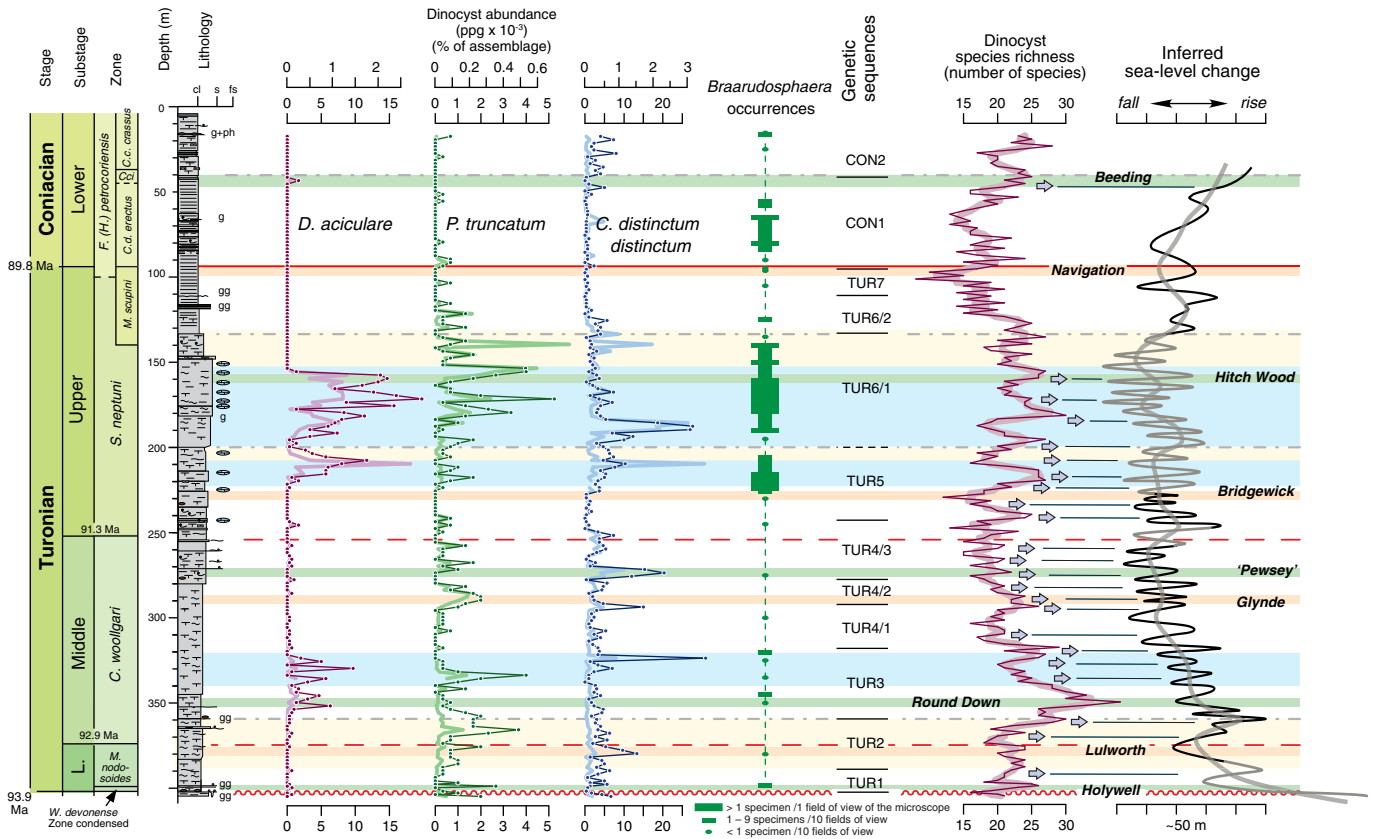
Fig. 11. Distribution of dinocyst species *D. aciculare*, *P. truncatum* and *C. distinctum distinctum*, which have been judged to reflect low salinity/more proximal environments, and correlation between species richness and relative sea-level trends. Thicker lines show absolute abundance of dinocysts (specimens per gram of the non-carbonate fraction of the sediment), while thinner lines and points show percentage of the dinocyst assemblage. Distribution of the proximal-indicating nannofossil species *Braarudosphaera* is also indicated. Arrows and tie lines show coincidence between increases in species richness and inflection points (flooding events) on the relative sea-level curve.

to one comprising solely of lower-salinity forms, and the high diversity reflects this. Diversity maxima coincident with major transgressions, indicate maximum offshore transport of near-shore taxa during flooding. As diversity begins to decrease towards the top of TUR6/2, there is a short peak in abundance, driven by G- rather than P-cysts, before a decline to low abundances up to the Turonian–Coniacian boundary. An Upper Turonian abundance peak followed by an uppermost Turonian abundance minimum has also been recorded in Norfolk, England (Pearce, 2000).

4.2.3. Turonian–Coniacian boundary

Following the cyclic diversity variations in TUR5 and 6/1, there is a decline through TUR6/2 and TUR7 to a minimum immediately below the Turonian–Coniacian boundary. The assemblage at this point again comprises outer-shelf normal-marine species, with an increasing abundance of the P-cyst *P. infusorioides*. This may be related to a decline in proximal influence, evidenced by the facies change to finer gained mudrocks, and the re-initiation of upwelling in the area. The dinocyst abundance peak and subsequent sharp decline noted above the Turonian–Coniacian boundary is coincident with abundance peaks, particularly of *P. infusorioides*, found in UK sections (Pearce, 2000; Olde et al., 2015). In the BGS Trunch borehole, Norfolk, a peak in P/G ratio occurs immediately above the Turonian–Coniacian boundary. The maximum in total dinocyst abundance follows the P/G maximum, so a mixture of P- and G-cysts drives abundance. An abundance decline is then recorded in the Lower Coniacian. In Berkshire, the Upper Turonian is very condensed compared to Bch-1 and Norfolk, hampering comparison, but a decline in abundance is found spanning the Turonian–Coniacian boundary, albeit beginning earlier than in Bch-1 and Norfolk (Pearce et al., 2003).

Reasonable agreement exists through the Turonian part of the core between occurrences of proximal-indicating dinocyst species, such as *Circulodinium*, and the nannofossil *Braarudosphaera* (Fig. 11). However, in the lowest Coniacian *C. d. erectus* Zone, *Braarudosphaera* occurs with no corresponding peak in *Circulodinium*. It instead coincides with a large peak in the abundance of P-cyst *P. infusorioides*, high P/G ratios, and a diversity minimum, together indicative of eutrophic conditions. Blooms of *Braarudosphaera* in the Turonian have been correlated not just to lowered salinity and near-shore environments, but also to eutrophication (Cunha and Shimabukuro, 1997). It could therefore be the case that in this part of the section, *Braarudosphaera* is responding not to salinity and sea level, but to the nutrient input that is also driving high numbers of *P. infusorioides*.

Dinocyst diversity increases again in the Lower Coniacian. This diversity increase is not accompanied by an increase in inner neritic taxa, as with the earlier diversity maxima (Figs. 7, 11), but is instead driven by more consistent records of taxa that occur only sporadically lower in the core. As this is coincident with a sharp decline in P/G ratio and in the abundance of dinocysts, it probably reflects the eustatic sea-level rise that began around the stage boundary. The environment is interpreted to be a eutrophic deeper shelf. The increasing diversity of 'oceanic' species could be due to flooding of the northerly barrier, and broadening of the 'Elbe Strait' gateway allowing greater exchange with the Boreal Sea. The appearance of common *Chatangiella* and *Isabelidinium*, which are abundant in the Turonian–Coniacian of Greenland and the North Sea Basin (Nøhr-Hansen, 1996), supports this theory.

Southward shifts of cool water masses into Europe has been previously recognised from the migrations of ammonites and echinoids coincident with positive shifts in δ18O in the Upper Turonian and Lower

Coniacian (Voigt and Wiese, 2000). *Chatangiella* is first recorded at the top of TUR6/1 coincident with the facies change marking *M. scupini* Zone flooding. The genus then becomes uncommon during the latest Turonian lowstand (basal Sequence CON1), before increasing progressively again with Coniacian sea-level rise in CON1. Other dinocyst species that become more frequent in the upper part of the core include *Surculosphaeridium longifurcatum*, *Exochosphaeridium arnace*, *Cribroperidinium wilsonii* and *Surculosphaeridium belowii*.

4.2.4. Dinocyst species richness and sea-level change

The strong similarity between long-term trends in the dinocyst species richness and $\delta^{13}C_{org}$ curves is notable (Fig. 10). This is not driven by the abundance of palynomorphs, as there is no correspondence with the abundance trends (Fig. 9). Correlation between the $\delta^{13}C_{org}$ curve for Bch-1 and the $\delta^{13}C$ carbonate reference curve of Jarvis et al. (2006) discussed in detail by Uličný et al. (2014), suggests that the $\delta^{13}C_{org}$ curve presented closely reflects global $\delta^{13}C$ trends. Additionally, long-term (≥ 1 Myr scale) highs and lows in $\delta^{13}C$ appear to roughly correspond to intervals characterized by more pronounced short-term sea-level highs and lows, respectively.

A long-term relationship between global dinocyst diversity and eustatic sea level has been previously suggested (Fig. 1; MacRae et al., 1996; Fensome et al., 1997; Sluijs et al., 2005). In terms of inshore to offshore trends, the expected pattern would be to see an increase in diversity and a decline in absolute abundance accompanying sea-level rise, representing the transition from a near-shore to a deeper water environment with lower nutrient availability. However, this is not the case in Bch-1 for Upper Turonian Sequence TUR6/1, where a positive correlation between species diversity and $\delta^{13}C_{org}$ accompanies moderately rising dinocyst abundances within an interval of long-term regional sea-level fall. Rather than high sea level, the diversity maximum may instead be generated here by the mixing of near-shore and outer-shelf assemblages by rapid T–R cycles in generally shallow water, with hypopycnal flows reaching the central basin during lowstands, but having the greatest influence during episodes of short- to medium-term sea-level rise. Changes in palaeocirculation and the opening of gateways during flooding events may also be important drivers of diversity within this basin.

To further investigate links between $\delta^{13}C$, sea level and dinocyst diversity, additional sections in the Bohemian Cretaceous Basin and in basins in other parts of the world will need to be examined.

4.2.5. Palaeoproductivity and long-term sea-level change

The dinocyst P/G ratio, controlled largely by variation in the abundance of *P. infusorioides* provides a productivity proxy. A long-term rise in P/G ratios during the Early to early Late Turonian is consistent with enhanced nutrient availability derived from stronger terrigenous input accompanying sea-level fall. However, there is no obvious relationship between the abundance of peridinioid cysts and terrestrial-run-off proxies, such as terrestrial palynomorph abundance, T/M index or Ti/Al ratios. A crash in *P. infusorioides* abundance at the onset of the main long-term Late Turonian lowstand indicates sharply decreased productivity during the period of lowest sea level. Renewed productivity accompanied the onset of Early Coniacian rapid sea-level rise; a distinctive acme of *P. infusorioides* at this time is also recognized in eastern England.

Average palaeowater depths for the central basin setting of the core site are believed to have fluctuated through time between ~50–60 m and a maximum of >100 m (Mitchell et al., 2010). The shoal area of the 'Elbe Strait' is estimated to have been <35 m deep (Fig. 2). During the Turonian, short-term cycles of sea-level fall estimated to be in the order of 20 m or less, were superimposed on a pattern of long-term sea-level fall and rise of approximately 50 m maximum, as suggested by Uličný et al. (2009) and unpublished data. Oceanic depth of >2000 m characterized the eastern part of the Penninic Ocean, to the southeast of the Bohemian Cretaceous Basin. To the north, the basin was

connected to the Boreal Sea through fault-controlled straits separating the Most-Teplice High and Sudetic Islands. These northern straits were tidally dominated (Mitchell et al., 2010), and it is likely that the western 'Elbe Strait' gateway was closed with sea-level fall and delta progradation during maximum sea-level lowstands of the Early to early Middle Turonian, and although permanently drowned during the later Turonian–Coniacian, may have narrowed with reduced water exchange during later lowstand intervals.

Assuming a largely terrestrial source of nutrients, reduced productivity during the long-term Late Turonian lowstand might be due to: (1) sea level falling below a minimum water depth threshold required to support optimum dinoflagellate primary production and/or encystment in the study area. Onshore-offshore turbidity and salinity gradients would likely play important roles, and increased surface-water turbidity and reduced light penetration associated with hypopycnal flows might be expected to lower surface productivity, despite increased nutrient supply; (2) lower terrestrial nutrient fluxes caused by reduced rates of weathering, low pCO_2 (Hasegawa, 2003; Uramoto et al., 2013) and cooling during the Late Turonian climate event (cf. Voigt, 2000; Voigt and Wiese, 2000; Voigt et al., 2004).

Modelling (Poulsen et al., 1999; Fluteau et al., 2007) and geological data from the mid-Cretaceous erg in Spain (Rodríguez-López et al., 2008) both indicate that the Bohemian Cretaceous Basin was situated in a belt of prevailing westerly winds. This offers potential to drive offshore Ekman transport of surface waters away from the northern island system and initiate a local coastal upwelling system (cf. Pearce et al., 2009), with increased marine productivity supported by the influx of nutrients from the Penninic Ocean to the SE (Fig. 2). The potential to develop an upwelling system with subsurface water input from the open ocean might have been limited by water depth and topographic restriction across the Králíky Shoal, particularly during sea-level lowstands. However, the width and palaeodepth of the shaol area is poorly constrained due to a lack of preserved sediments. Moreover, the shoal was drowned by the early Middle Turonian, which would have allowed greater water mass exchange thereafter. The early Late Turonian productivity crash might be attributable to the temporary breakdown of the upwelling system, which became re-established during Late Turonian–Coniacian sea-level rise.

Despite uncertainties concerning nutrient sources, it is postulated that sea level played a critical role in controlling the palynological assembles at Bch-1. Long-term Turonian eustatic sea-level fall caused the Bch-1 study site to become influenced by progressively shallower water conditions, driving major changes in palynological assemblages, as the site moved from a central basin setting, through an offshore high productivity zone, into shallower water areas highly influenced by hypopycnal flows (Fig. 12). Early Coniacian sea-level rise reversed the earlier trends.

4.2.6. T/M index as a sea-level proxy

Terrestrial palynomorph abundance and T/M index values display variable relationships to T/R max / shore proximity curves and in this type of environment cannot be regarded in isolation as reliable sea-level proxies. High T/M ratios characterize the main long-term regressive package of the Upper Turonian and some short-term peaks correspond to regressive maxima, but elsewhere in the succession high abundances and/or ratios are recorded during periods of falling or rising sea level.

5. Conclusions

Elemental chemostratigraphy provides a reliable means of identifying long- (1–2 Myr) to medium-term (0.4–1 Myr) sea-level trends in Cretaceous hemipelagic successions. Maxima in bulk sediment manganese content are associated with maximum flooding zones, and troughs with intervals of lowstand. Falling Mn contents accompany regression
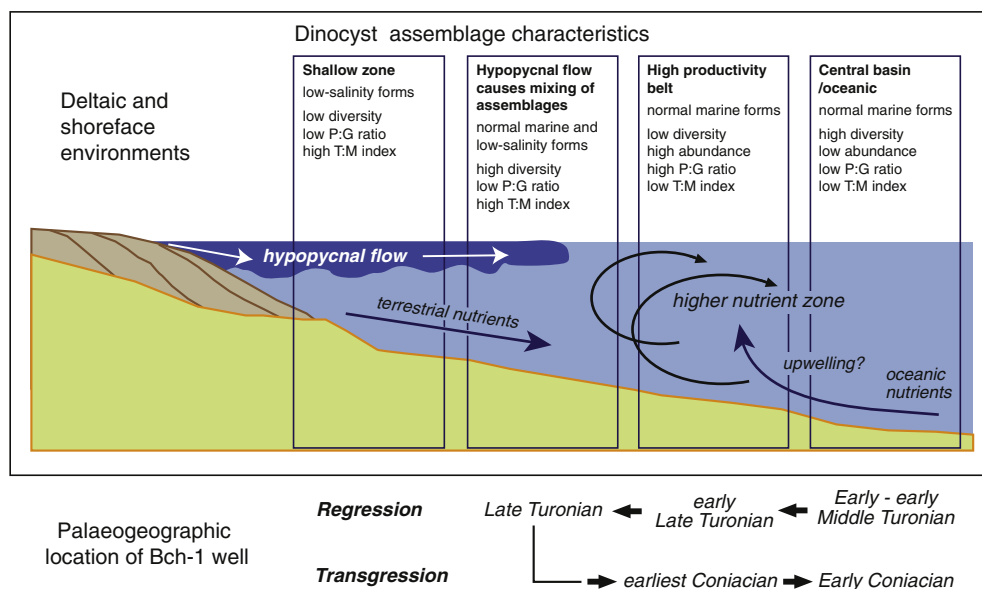
Fig. 12. Generalised palaeoenvironments and long-term sea-level changes producing variation in palynological assemblages through the Bch-1 core. For simplicity, the Early Turonian regression and other medium- to short-term sea-level cycles are not represented.

and rising values transgression. Rising Si/Al, Ti/Al and Zr/Al ratios accompany long-term sea-level fall, and declining values sea-level rise. Transgressive events associated with medium-term sea-level change are marked by sharp increases in Ti/Al ratios, supplemented by Si/Al and Zr/Al peaks of varying amplitude. However, smaller scale short-term (100 kyr) sea-level variation is not fully resolved by chemostratigraphic profiles.

Long-term 'background' (2.4 Myr) and shorter-term (1 Myr scale) highs and lows in $\delta^{13}C_{org}$ closely follow trends in dinocyst species richness. Highs and lows in both parameters broadly correspond to intervals characterised by more pronounced short-term sea-level highs and lows, respectively. Lower Middle Turonian (Round Down CIE) and Upper Turonian (~Hitch Wood CIE) maxima, and basal Upper Turonian and Turonian–Coniacian boundary minima (Bridgewick and Navigation CIEs) occur in both proxies. Baseline trends have a cycle duration close to the 2.4 Myr long-eccentricity cycle. These trends are consistent with the concepts of rising eustatic sea-level driving increased global organic carbon burial, and of increasing dinocyst diversity accompanying increasing shelf area. However, on the scale of intermediate- to short-term $\delta^{13}C$ fluctuations, no systematic relationship between $\delta^{13}C$ and sea-level change can be demonstrated.

Dinocyst species richness closely follows short-term (100 kyr) changes in sea level, with marked increases in dinocyst diversity coincident with each short-term flooding event, particularly in the Middle Turonian. Periods of rapid sea-level rise caused an influx of a more diverse 'outer shelf' assemblage into the study area, together with the addition of shallower water species, some of which were likely transported into the central basin by hypopycnal flows.

Dinocyst species richness provides an excellent sea-level proxy in the Bohemian Cretaceous Basin. Low-diversity dinocyst assemblages in basinal sediments correlate to sea-level minima. Sharp increases in species richness accompany transgression, with maxima during periods of maximum flooding. Fourteen out of 18 well-defined short-term transgressive-regressive sea-level cycles in the Middle–Upper Turonian are clearly expressed by peaks and troughs in the dinocyst species richness record.

Early Middle Turonian sea-level fall may have temporarily led to the restriction or closure of the NW connection of the Bohemian Cretaceous Basin to the northern Europe Boreal Sea via the 'Elbe Strait' gateway.

Increasing diversity of oceanic dinocyst species in the earliest Coniacian might be due to re-opening of the 'Elbe Strait' gateway allowing greater exchange with the Boreal Sea, evidenced by the appearance of common northern-affinity dinocyst taxa.

Changes in the proportion of peridinioid dinoflagellate cysts (particularly *P. infusorioides*), considered to be the product of heterotrophic dinoflagellates, were likely controlled principally by changing nutrient levels. High peridinioid/gonyaulacoid (P/G) ratios correlate to intervals of low species richness and low T/M index. There is no consistent relationship between the abundance of peridinioid cysts and terrestrial-run-off proxies. This, along with the association of *P. infusorioides* with mid- to outer shelf dinocyst species, suggests that upwelling rather than terrestrially derived nutrients drove organic-walled phytoplankton productivity in the Bohemian Cretaceous Basin.

Neither the proportion nor abundance of terrestrial palynomorphs in the sediment proves to be a reliable sea-level proxy. Only a weak correlation exists between variation in the terrestrial/marine (T/M) palynomorph index and sea-level change. An interval of long-term low sea level in the Upper Turonian is characterised by increased T/M ratios, with peaks in T/M index corresponding to intervals of medium-term sea-level fall. However, a Lower Turonian regressive package shows no increase in T/M index, but a major peak occurs above, immediately following a highstand, while in the Lower Coniacian, rising sea levels are marked by rising not falling T/M ratios.

Multidisciplinary records show that proximity proxies from palynological and geochemical data are not always consistent, exemplifying the need for understanding the provenance and dispersal patterns of siliciclastic sediments, and factors influencing palynological proxies such as changes in water mass circulation, before making simplistic sea level interpretations. Although increases in dinoflagellate cyst diversity are often observed when travelling from near- to offshore, in the Bohemian Basin some increases in diversity include additions of species with near-shore affinities. This demonstrates the need for a greater understanding of the palaeoenvironmental preferences of dinoflagellate species before making interpretations based purely on abundance and diversity trends. In the case of the Bohemian Basin, palynological assemblages appear to have been influenced by changes in both water mass circulation and input from hypopycnal flows.

Acknowledgments

Appendix A. Species list

Complete list of dinoflagellate cyst species recorded in the Bch-1 core. Numbers correspond to the order of species plotted in Appendix B. Other taxa, found less commonly, are also listed along with the genetic sequence(s) from which they have been identified (i.e. TUR1–7, CON1–2, Fig. 3). Taxonomic references are given in Fensome et al. (2008) and Pearce et al. (2011).

26	*Achomosphaera ramulifera ramulifera* (Deflandre 1937) Evitt 1963
33	*Achomosphaera regiensis* Corradini 1973
1	*Achomosphaera sagena* Davey and Williams 1966
2	*Callaiosphaeridium asymmetricum* (Deflandre and Courteville 1939) Davey and Williams 1966
41	*Cassiculosphaeridia reticulata* Davey 1969
22	*Cauveridinium membraniphorum–Cyclonephelium compactum* Complex of Marshall and Batten, 1988
58	*Chatangiella ditissima* (McIntyre 1975) Lentin and Williams 1976
3	*Circulodinium distinctum distinctum* (Deflandre and Cookson 1955) Jansonius 1986
39	*Circulodinium latoaculeum* (Yun Hyesu 1981) Islam 1993
TUR3	*Cometodinium obscurum* Deflandre and Courteville 1939
59	*Cometodinium whitei* (Deflandre and Courteville 1939) Stover and Evitt 1978
CON1, 2	*Conosphaeridium* Cookson and Eisenack 1969
CON1	*Conosphaeridium striatoconum* (Deflandre and Cookson 1955) Cookson and Eisenack 1969
4	*Coronifera oceanica* Cookson and Eisenack 1958
5	*Cribroperidinium orthoceras* (Eisenack 1958) Davey 1969
70	*Cribroperidinium* sp. Neale and Sarjeant 1962
76	*Cribroperidinium wilsonii* (Yun Hyesu 1981) Poulsen 1996
73	*Cyclonephelium filoreticulatum* (Slimani 1994) Prince et al., 1999
TUR6/1, CON2	*Cyclonephelium hughesii* Clarke and Verdier 1967
31	*Dapsilidinium laminaspinosum* (Davey and Williams 1966) Lentin and Williams 1981
72	*Dinogymnium acuminatum* Evitt *et al.* 1967
27	*Dinopterygium cladoides* Deflandre 1935
40	*Disphaeria macropyla* Eisenack and Cookson 1960
23	*Downiesphaeridium aciculare* (Davey 1969) Islam 1993
42	*Downiesphaeridium armatum* (Deflandre 1937) Islam 1993
37	*Ellipsodinium rugulosum* Clarke and Verdier 1967
24	*Exochosphaeridium arnace* Davey and Verdier 1973
43	*Exochosphaeridium bifidum* (Clarke and Verdier 1967) Clarke *et al.* 1968
60	*Exochosphaeridium phragmites* Davey *et al.* 1966
67	*Florentinia buspina* (Davey and Verdier 1976) Duxbury 1980
71	*Florentinia clavigera* (Deflandre 1937) Davey and Verdier 1973
28	*Florentinia cooksoniae* (Singh 1971) Duxbury 1980
47	*Florentinia laciniata* Davey and Verdier 1973
7	*Florentinia mantellii* (Davey and Williams 1966) Davey and Verdier 1973

34	*Florentinia* sp. Davey and Verdier 1973
8	*Hystrichodinium pulchrum* Deflandre 1935
TUR4/1	*Hystrichosphaeridium* sp. Deflandre 1937
32	*Hystrichosphaeridium bowerbankii* Davey and Williams 1966
49	*Hystrichosphaeridium conispiniferum* Yun Hyesu 1981
9	*Hystrichosphaeridium recurvatum* (White 1842) Lejeune-Carpentier, 1940
50	*Hystrichosphaeridium salpingophorum* Deflandre 1935
10	*Hystrichosphaeridium tubiferum tubiferum* (Ehrenberg 1838) Deflandre 1937
63	*Hystrichosphaeridium tubiferum brevispinum* (Davey and Williams 1966) Lentin and Williams 1993
52	*Hystrichostrogylon membraniphorum* Agelopoulos 1964
69	*Impletosphaeridium clavulum* (Davey 1969) Islam 1993
74	*Isabelidinium?* *amphiatum* (McIntyre 1975) Lentin and Williams 1977
TUR4/1	*Kallosphaeridium?* *ringnesiorum* (Manum and Cookson 1964) Helby 1987
54	*Kiokansium unituberculatum* (Tasch in Tasch et al. 1964) Stover & Evitt 1978
35	*Kleithriasphaeridium loffrense* Davey and Verdier 1976
11	*Kleithriasphaeridium readei* (Davey and Williams 1966) Davey and Verdier 1976
TUR6/1, CON2	*Litosphaeridium arundum* (Eisenack and Cookson 1960) Davey 1979; emend. Lucas-Clark 1984
36	*Membranilarnacia polycladiata* Cookson and Eisenack in Eisenack 1963
29	*Microdinium distinctum* Davey 1969
55	*Nematosphaeropsis denseradiata* (Cookson and Eisenack 1962) Stover and Evitt 1978
45	*Odontochitina costata* Alberti 1961; emend. Clarke and Verdier 1967
12	*Odontochitina operculata* (Wetzel 1933a) Deflandre and Cookson 1955
53	*Odontochitina singhii* Morgan 1980
TUR4/1	*Odontochitinopsis molesta* (Deflandre 1937) Eisenack 1961
13	*Oligosphaeridium complex* (White 1842) Davey and Williams 1966
48	*Oligosphaeridium poculum* Jain 1977
14	*Oligosphaeridium prolixispinosum* Davey and Williams 1966
46	*Oligosphaeridium pulcherrimum* (Deflandre and Cookson 1955) Davey and Williams 1966
15	*Palaeohystrichophora infusorioides* Deflandre 1935
CON1	*Pareodinia ceratophora* Deflandre 1947
TUR2	*Pervosphaeridium* sp. Yun Hyesu 1981
TUR2–4/1, 4/3	*Pervosphaeridium cenomaniense* (Norvick 1976) Below 1982
TUR3–4/1, CON1	*Pervosphaeridium monasteriense* Yun Hyesu 1981
64	*Pervosphaeridium pseudhystrichodinium* (Deflandre 1937) Yun Hyesu 1981
16	*Pervosphaeridium truncatum* (Davey 1969) Below 1982
17	*Prolixosphaeridium granulosum* (Deflandre 1937) Davey et al. 1966
18	*Pterodinium "crassimuratum"* (Davey and Williams 1966) Thurow *et al.* 1988
68	*Raetiaedinium truncigerum* (Deflandre 1937) Kirsch 1991
CON1	*Scriniodinium campanula* Gocht 1959
44	*Senoniasphaera turonica* (Prössl, 1990 ex Prössl, 1992) Pearce et al., 2011
62	*Sentusidinium* sp. Sarjeant and Stover 1978
6	*Sepispinula?* *ambigua* (Deflandre 1937) Masure in Fauconnier and Masure 2004
38	*Spiniferites membranaceus* (Rossignol 1964) Sarjeant 1970
25	*Spiniferites ramosus granosus* (Davey and Williams 1966) Lentin and Williams 1973
19	*Spiniferites ramosus ramosus* (Ehrenberg 1838) Mantell 1854

51	*Stephodinium coronatum* Deflandre 1936

51 *Stephodinium coronatum* Deflandre 1936

56 *Subtilisphaera pontis-mariae* (Deflandre 1936) Lentin and Williams 1976

TUR3, 4/1 *Surculosphaeridium? basifurcatum* Yun Hyesu 1981

75 *Surculosphaeridium belowii* Yun Hyesu 1981

20 *Surculosphaeridium longifurcatum* (Firtion 1952) Davey *et al.* 1966

21 *Tanyosphaeridium salpinx* Norvick 1976

61 *Tanyosphaeridium variecalamum* Davey and Williams 1966

65 *Tenua hystrix* Eisenack 1958

30 *Trichodinium castanea* Deflandre 1935

57 *Wrevittia* cf. *cassidata* (Eisenack and Cookson 1960) Helenes and Lucas-Clark 1997

TUR4/1 *Wrevittia helicoidea* (Eisenack and Cookson 1960) Helenes and Lucas-Clark 1997

TUR4/3–6/2 *Xenascus ceratioides* (Deflandre 1937) Lentin and Williams 1973

66 *Xiphophoridium asteriforme* Yun Hyesu 1981

Appendix B. Supplementary data

Dinocyst range chart and elemental data. Supplementary data associated with this article can be found, in the online version, at http://dx.doi.org/10.1016/j.palaeo.2015.06.018. These data include Google map of the most important areas described in this article.

References

Ando, A., Huber, B.T., MacLeod, K.G., Ohta, T., Khim, B.K., 2009. Blake Nose stable isotopic evidence against the mid-Cenomanian glaciation hypothesis. Geology 37, 451–454.
Batten, D.J., 1982. Palynofacies and salinity in the Purbeck and Wealden of southern England. In: Banner, F.T., Lord, A.R. (Eds.), Aspects of Micropalaeontology. George Allen & Unwin, London, pp. 278–308.
Bertrand, P., Shimmield, G., Martinez, P., Grousset, F., Jorissen, F., Paterne, M., Pujol, C., Bouloubassi, I., Menard, P.B., Peypouquet, J.P., Beaufort, L., Sicre, M.A., LallierVerges, E., Foster, J.M., Ternois, Y., 1996. The glacial ocean productivity hypothesis: The importance of regional temporal and spatial studies. Mar. Geol. 130, 1–9.
Bint, A.N., 1988. Recent dinoflagellate cysts from Mermaid Sound northwestern Australia. In: Jell, P.A., Playford, G. (Eds.), Palynological and Palaeobotanical Studies in Honour of Basil E. Balme, pp. 329–341.
Bornemann, A., Norris, R.D., Friedrich, O., Beckmann, B., Schouten, S., Damste, J.S.S., Vogel, J., Hofmann, P., Wagner, T., 2008. Isotopic evidence for glaciation during the Cretaceous supergreenhouse. Science 319, 189–192.
Bradford, M.R., Wall, D.A., 1984. The distribution of recent organic walled dinoflagellate cysts in the Persian Gulf of Oman and northwestern Arabian Sea. Palaeontogr. Abt. B Palaeophytol. 192, 16–84.
Brinkhuis, H., Zachariasse, W.J., 1988. Dinoflagellate cysts, sea-level changes and planktonic foraminifers across the Cretaceous–Tertiary boundary at El Haria, northwest Tunisia. Mar. Micropaleontol. 13, 153–191.
Bujak, J.P., Williams, G.L., 1979. Dinoflagellate diversity through time. Mar. Micropaleontol. 4, 1–12.
Bukry, D., 1974. Coccoliths as paleosalinity indicators: evidence from the Black Sea. In: Degens, E.T., Ross, D.R. (Eds.), The Black Sea - Geology, Chemistry, and Biology. American Association of Petroleum Geologists, Tulsa, pp. 303–327.
Burnett, J.A., Gallagher, L.T., Hampton, M.J., 1998. Upper Cretaceous. In: Bown, P.R. (Ed.), Calcareous Nannofossil Biostratigraphy. Kluwer, Dordrecht, pp. 132–199.
Catuneanu, O., Galloway, W.E., Kendall, C.G.S.C., Miall, A.D., Posamentier, H.W., Strasser, A., Tucker, M., 2011. Sequence stratigraphy: Methodology and nomenclature. Newsl. Stratigr. 44, 173–245.
Čech, S., Klein, V., Kříž, J., Valečka, J., 1980. Revision of the Upper Cretaceous stratigraphy of the Bohemian Cretaceous Basin. Věstník Ústředního Ústavu Geologického (Bulletin of the Geological Survey) 55 pp. 277–296.
Čech, S., Hradecká, L., Svobodová, M., Švábenická, L., 2005. Cenomanian and Cenomanian-Turonian boundary in the southern part of the Bohemian Cretaceous Basin, Czech Republic. Bull. Geosci. 80, 321–354.
Chen, H.-F., Yeh, P.-Y., Song, S.-R., Hsu, S.-C., Yang, T.-N., Wang, Y., Chi, Z., Lee, T.-Q., Chen, M.-T., Cheng, C.-L., Zou, J., Chang, Y.-P., 2013. The Ti/Al molar ratio as a new proxy for tracing sediment transportation processes and its application in aeolian events and sea level change in East Asia. J. Asian Earth Sci. 73, 31–38.
Corbin, J.C., Person, A., Iatzoura, A., Ferre, B., Renard, M., 2000. Manganese in pelagic carbonates: indication of major tectonic events during the geodynamic evolution of a passive continental margin (the Jurassic European margin of the Tethys-Ligurian Sea). Palaeogeogr. Palaeoclimatol. Palaeoecol. 156, 123–138.
Costa, L., Davey, R.J., 1992. Dinoflagellates of the Cretaceous System. In: Powell, A.J. (Ed.), A Stratigraphic Index of Dinoflagellate Cysts. Chapman and Hall, pp. 99–153.

Cunha, A.S., Shimabukuro, S., 1997. *Braarudosphaera* blooms and anomalous enrichments of *Nannoconus*: evidence from the Turonian South Atlantic, Santos Basin. Brazil. J. Nannoplankton Res. 19, 51–55.
Dale, B., 1992. Chapter 1. Dinoflagellate contributions to the open marine flux. In: Dale, B., Dale, A.L. (Eds.), Dinoflagellate Contributions to the Deep Sea. Woods Hole Oceanographic Institution, Woods Hole Massachusetts, pp. 1–32.
Rojas de Mandiola, B., 1981. Seasonal phytoplankton distribution along the Peruvian coast. In: Richards, F.A. (Ed.), Coastal Upwelling. American Geophysical Union, pp. 348–356.
de Rafélis, M., Emmanuel, L., Renard, M., Atrops, F., Du Chene, R.J., 2001. Geochemical characterization (Mn content) of third order eustatic sequences in Upper Jurassic pelagic carbonates of the Vocontian Trough (SE France). Eclogae Geol. Helv. 94, 145–152.
de Vernal, A., Mudie, P.G., 1989. Pliocene and Pleistocene palynostratigraphy at ODP Sites 646 and 647, eastern and southern Labrador Sea. In: Srivastava, S.P., Arthur, M.A., Clement, B., Aksu, A., Baldauf, J., Bohrman, G., Busch, W., Cederberg, T., Cremer, M., Dadey, K., de Vernal, A., Firth, J., Hall, F., Head, M., Hiscott, R., Jarrard, R., Kaminiski, M., Lazarus, D., Monjanel, A.-L., Nielsen, O.B., Stein, R., Thiebault, F., Zachos, J.C., Zimmerman, H. (Eds.), Baffin Bay and Labrador Sea. Ocean Drilling Program, College Station TX, pp. 401–422.
Dodsworth, P., 2000. Trans-Atlantic dinoflagellate cyst stratigraphy across the Cenomanian–Turonian (Cretaceous) Stage boundary. J. Micropalaeontol. 19, 69–84.
Fensome, R.A., MacRae, R.A., Williams, G.L., 1997. Dinoflagellate evolution and diversity through time. Bedford Institute of Oceanography Science Review 1994 – 1995. Department of Fishereries and Oceans, aritimes Region, Ottawa Canada, pp. 45–50.
Fensome, R.A., MacRae, R.A., Williams, G.L., 2008. DINOFLAJ2, Version 1. Am. Assoc. Stratigraphic Palynologists, Data Ser. 937.
Floegel, S., Wallmann, K., Kuhnt, W., 2011. Cool episodes in the Cretaceous - Exploring the effects of physical forcings on Antarctic snow accumulation. Earth Planet. Sci. Lett. 307, 279–288.
Fluteau, F., Ramstein, G., Besse, J., Guiraud, R., Masse, J.P., 2007. Impacts of palaeogeography and sea level changes on mid-Cretaceous climate. Palaeogeogr. Palaeoclimatol. Palaeoecol. 247, 357–381.
Foucher, J.-C., 1981. Kystes de Dinoflagellés du Crétacé moyen européen: Proposition d'une échelle biostratigraphique pour le domaine nord-occidental. Cretac. Res. 2, 331–338.
Friedrich, O., Norris, R.D., Erbacher, J., 2012. Evolution of middle to Late Cretaceous oceans - A 55 m.y. record of Earth's temperature and carbon cycle. Geology 40, 107–110.
Gale, A.S., 1996. Turonian correlation and sequence stratigraphy of the Chalk in southern England. In: Hesselbo, S.P., Parkinson, D.N. (Eds.), Sequence Stratigraphy in British Geology. Geological Society of London, Bath, pp. 177–195.
Garrison, D., Buck, K.R., Gowing, M.M., 1991. Plankton assemblages in the ice edge zone of the Weddell Sea during austral winter. J. Mar. Syst. 2, 123–130.
Gradstein, F.M., Ogg, J.G., Schmitz, M.D., Ogg, G.M., 2012. The Geologic Time Scale 2012. Elsevier, Amsterdam (1144 pp.).
Gröcke, D.R., Ludvigson, G.A., Witzke, B.L., Robinson, S.A., Joeckel, R.M., Ufnar, D.F., Ravn, R.L., 2006. Recognizing the Albian–Cenomanian (OAE1d) sequence boundary using plant carbon isotopes: Dakota Formation, Western Interior Basin, USA. Geology 34, 193–196.
Habib, D., Moshkovitz, S., Kramer, C., 1992. Dinoflagellate and calcareous nannofossil response to sea-level change in Cretaceous–Tertiary boundary sections. Geology 20, 165–168.
Hancock, J.M., Kauffman, E.G., 1979. The great transgressions of the Late Cretaceous. J. Geol. Soc. Lond. 136, 175–186.
Haq, B.U., 2014. Cretaceous eustasy revisited. Glob. Planet. Chang. 113, 44–58.
Haq, B.U., Al-Qahtani, A.M., 2005. Phanerozoic cycles of sea-level change on the Arabian Platform. Geophys. J. R. Astron. Soc. 10, 127–160.
Haq, B.U., Hardenbol, J., Vail, P.R., 1987. Chronology of fluctuating sea levels since the Triassic. Science 235, 1156–1167.
Harker, S.D., Sarjeant, W.A.S., Caldwell, W.G.E., 1990. Late Cretaceous (Campanian) organic-walled microplankton from the interior plains of Canada, Wyoming and Texas: biostratigraphy, palaeontology and palaeoenvironmental interpretation. Palaeontogr. Abt. B 219 (243 pp.).
Harland, R., 1973. Dinoflagellate cysts and acritarchs from the Bearpaw Formation (Upper Campanian) of southern Alberta, Canada. Palaeontology 16, 665–706.
Harris, A.J., Tocher, B.A., 2003. Palaeoenvironmental analysis of Late Cretaceous dinoflagellate cyst assemblages using high-resolution sample correlation from the Western Interior Basin. Mar. Micropaleontol. 48, 127–148.
Hasegawa, T., 2003. Cretaceous terrestrial paleoenvironments of northeastern Asia suggested from carbon isotope stratigraphy: increased atmospheric pCO$_2$-induced climate. J. Asian Earth Sci. 21, 849–859.
Helenes, J., Somoza, D., 1999. Palynology and sequence stratigraphy of the Cretaceous of eastern Venezuela. Cretac. Res. 20, 447–463.
Hunt, C., 1987. Dinoflagellate cyst and acritarch assemblages in shallow-marine and marginal marine carbonates: the Portland Sand, Portland Stone, and Purbeck Formation (Upper Jurassic/Lower Cretaceous) of southern England and northern France. In: Hart, M.B. (Ed.), The Micropalaeontology of Carbonate Environments. Ellis Horwood, Chichester, pp. 208–225.
Imai, N., Terashima, S., Itah, S., Ando, A., 1996. 1996 compilation of analytical data on nine GSJ geochemical reference samples, "sedimentary rock series". Geostand. Newslett. 20, 165–216.
Jarvis, I., 2003. Sample preparation in ICP-MS. In: Jarvis, K.E., Gray, A.L., Houk, R.S. (Eds.), Handbook of Inductively Coupled Plasma Mass Spectrometry. Viridian, Woking, pp. 172–224.
Jarvis, I., Murphy, A.M., Gale, A.S., 2001. Geochemistry of pelagic and hemipelagic carbonates: criteria for identifying systems tracts and sea-level change. J. Geol. Soc. Lond. 158, 685–696.

Jarvis, I., Mabrouk, A., Moody, R.T.J., De Cabrera, S.C., 2002. Late Cretaceous (Campanian) carbon isotope events, sea-level change and correlation of the Tethyan and Boreal realms. Palaeogeogr. Palaeoclimatol. Palaeoecol. 188, 215–248.

Jarvis, I., Gale, A.S., Jenkyns, H.C., Pearce, M.A., 2006. Secular variation in Late Cretaceous carbon isotopes and sea-level change: evidence from a new δ13C carbonate reference curve for the Cenomanian–Campanian (99.6–70.6 Ma). Geol. Mag. 143, 561–608.

Jarvis, I., Mabrouk, A., Moody, R.T.J., Murphy, A.M., Sandman, R.I., 2008. Applications of carbon isotope and elemental (Sr/Ca, Mn) chemostratigraphy to sequence analysis: sea-level change and the global correlation of pelagic carbonates. In: Salem, M.J., El-Hawat, A.S. (Eds.), Geology of East Libya. Earth Science Society of Libya, Tripoli, pp. 369–396.

Jarvis, I., Trabucho-Alexandre, J., Gröcke, D., Uličný, D., Laurin, J., 2015. Stable-isotope chemostratigraphy: intercontinental correlation of organic carbon and carbonate records, and evidence of climate and sea-level change during the Turonian (Cretaceous). Geophys. Res. Abstr. 17 (EGU2015–11192-1).

Joo, Y.J., Sageman, B.B., 2014. Cenomanian to Campanian carbon isotope chemostratigraphy from the Western Interior Basin. J. Sediment. Res. 84, 529–542.

Klein, V., Müller, V., Valečka, J., 1979. Lithofazielle und paläogeographische Entwicklung des Böhmischen Kreidebeckens. In: Wiedmann, J. (Ed.), Aspekte der Kreide Europas. E. Schweizerbart'sche Verlagsbuchhandlung, Nägele & Obermiller, Stuttgart, pp. 435–446.

Kominz, M.A., Browning, J.V., Miller, K.G., Sugarman, P.J., Mizintseva, S., Scotese, C.R., 2008. Late Cretaceous to Miocene sea-level estimates from the New Jersey and Delaware coastal plain coreholes: an error analysis. Basin Res. 20, 211–226.

Konno, S., Harada, N., Narita, H., Jordan, R.W., 2007. Living Braarudosphaera bigelowii (Gran & Braarud) Deflandre in the Bering Sea. J. Nannoplankton Res. 29, 78–87.

Laurin, J., Čech, S., Uličný, D., Štaffen, Z., Svobodová, M., 2014. Astrochronology of the Late Turonian: implications for the behavior of the carbon cycle at the demise of peak greenhouse. Earth Planet. Sci. Lett. 394, 254–269.

Le Callonnec, L., Renard, M., De Rafélis, M., Minoletti, F., Beltran, C., Du Chene, R.J., 2014. Evolution of the trace element contents (Sr and Mn) of hemipelagic carbonates from the Zumaia Paleocene section (Gipuzkoa, Spain): implications for the knowledge of seawater chemistry during the Selandian. Bull. Soc. géol. France 185, 413–435.

Leereveld, H., 1995. Dinoflagellate cysts from the Lower Cretaceous Rio Argos succession (SE Spain). Lab. Palynol. Palaeobot. Contrib. Ser. Utrecht 2, 1–175.

Lewis, J., Dodge, J.D., Powell, A.J., 1990. Quaternary dinoflagellate cysts from the upwelling system offshore Peru, Hole 686B, ODP Leg 112. In: Suess, E., von Huene, R., Emeis, K.-C., Bourgois, J., Cruzado Castañeda, J.d.C, De Wever, P., Eglinton, G., Garrison, R., Greenberg, M., Paz, E.H., Hill, P., Ibaraki, M., Kastner, M., Kemp, A.E.S., Kvenvolden, K., Langridge, R., Lindsley-Griffin, N., Marsters, J., Martini, E., McCabe, R., Ocola, L., Resig, J., Sanchez Fernandez, A.W., Schrader, H.J., Thornburg, T., Wefer, G., Yamano, M. (Eds.), Peru Continental Margin. Ocean Drilling Program, College Station TX, pp. 323–328.

Lignum, J., 2009. Cenomanian (Upper Cretaceous) palynology and chemostratigraphy: dinoflagellate cysts as indicators of palaeoenvironmental and sea-level change. unpublished PhD thesis, School of Geography, Geology and the Environment, Kingston University London, Kingston upon Thames, UK, 582 p.

Lignum, J., Jarvis, I., Pearce, M.A., 2008. A critical assessment of standard processing methods for the preparation of palynological samples. Rev. Palaeobot. Palynol. 149, 133–149.

Lister, J.K., Batten, D.J., 1988. Stratigraphic and palaeoenvironmental distribution of Early Cretaceous dinoflagellate cysts in the Hurlands Farm Borehole, West Sussex, England. Palaeontogr. Abt. B 210, 9–89.

MacEachern, J.A., Pemberton, S.G., Gingras, M.K., Bann, K.L., 2010. Ichnology and facies models. In: James, N.P., Dalrymple, R.W. (Eds.), Facies Models 4. Geological Association of Canada, pp. 19–58.

MacRae, R.A., Fensome, R.A., Williams, G.L., 1996. Fossil dinoflagellate diversity, originations, and extinctions and their significance. Can. J. Bot. 74, 1687–1694.

Marshall, K.L., Batten, D.J., 1988. Dinoflagellate cyst associations in Cenomanian–Turonian "black shale" sequences of northern Europe. Rev. Palaeobot. Palynol. 54, 85–103.

Mason, B., Moore, C.B., 1982. Principles of Geochemistry. 4th ed. Wiley, New York (344 pp).

May, F.E., 1977. Functional morphology, paleoecology, and systematics of Dinogymnium tests. Palynology 1, 103–121.

May, F.E., 1980. Dinoflagellate cysts of the Gymnodiniaceae, Peridiniaceae, and Gonyaulacaceae from the Upper Cretaceous Monmouth Group Atlantic Highlands New-Jersey USA. Palaeontogr. Abt. B Palaeophytol. 172, 10–116.

Meyers, S.R., Siewert, S.E., Singer, B.S., Sageman, B.B., Condon, D.J., Obradovich, J.D., Jicha, B.R., Sawyer, D.A., 2012. Intercalibration of radioisotopic and astrochronologic time scales for the Cenomanian-Turonian boundary interval, Western Interior Basin, USA. Geology 40, 7–10.

Miller, K.G., Sugarman, P.J., Browning, J.V., Kominz, M.A., Hernandez, J.C., Olsson, R.K., Wright, J.D., Feigenson, M.D., Van Sickel, W., 2003. Late Cretaceous chronology of large, rapid sea-level changes: glacioeustasy during the greenhouse world. Geology 31, 585–588.

Miller, K.G., Wright, J.D., Browning, J.V., 2005. Visions of ice sheets in a greenhouse world. Mar. Geol. 217, 215–231.

Miller, K.G., Mountain, G.S., Wright, J.D., Browning, J.V., 2011. A 180-million-year record of sea level and ice volume variations from continental margin and deep-sea isotopic records. Oceanography 24, 40–53.

Mitchell, S.F., Paul, C.R.C., Gale, A.S., 1996. Carbon isotopes and sequence stratigraphy. In: Howell, J.A., Aitken, J.F. (Eds.), High Resolution Sequence Stratigraphy: Innovations and Applications. Geological Society of London, Bath, pp. 11–24.

Mitchell, A.J., Uličný, D., Hampson, G.J., Allison, P.A., Gorman, G.J., Piggott, M.D., Wells, M.R., Pain, C.C., 2010. Modelling tidal current-induced bed shear stress and palaeocirculation in an epicontinental seaway: the Bohemian Cretaceous Basin, Central Europe. Sedimentology 57, 359–388.

Monteil, E., 1993. Dinoflagellate cyst biozonation of the Tithonian and Berriasian of South-East France. Correlation with the sequence stratigraphy. Bull. Centres Recherches Explor. Prod. Elf-Aquitaine 17, 249–273.

Moriya, K., Wilson, P.A., Friedrich, O., Erbacher, J., Kawahata, H., 2007. Testing for ice sheets during the mid-Cretaceous greenhouse using glassy foraminiferal calcite from the mid-Cenomanian tropics on Demerara Rise. Geology 35, 615–618.

Mudie, P.J., Aksu, A.E., 1984. Paleoclimate of Baffin Bay from 300,000-year record of foraminifera, dinoflagellates and pollen. Nature 312, 630–634.

Nøhr-Hansen, H., 1996. Upper Cretaceous dinoflagellate cyst stratigraphy, onshore West Greenland. Grøn. Geol Unders Bull. 170, 1–104.

Ogg, J.G., Hinnov, L.A., Huang, C., 2012. Cretaceous. In: Gradstein, F.M., Ogg, J.G., Schmitz, M.D., Ogg, G.M. (Eds.), The Geological Time Scale 2012. Elsevier, Amsterdam, pp. 793–853.

Olde, K., Jarvis, I., Pearce, M.A., Uličný, D., Tocher, B.A., Trabucho-Alexandre, J., Gröcke, D., 2015. A revised northern European Turonian (Upper Cretaceous) dinoflagellate cyst biostratigraphy: integrating palynology and carbon isotope events. Rev. Palaeobot. Palynol. 213, 1–16.

Pearce, M.A., 2000. Palynology and Chemostratigraphy of the Cenomanian to Lower Campanian Chalk of Southern and Eastern England. Unpublished PhD thesis, School of Earth Sciences and Geography, Kingston University London, Kingston upon Thames, UK, 432 p.

Pearce, T.J., Jarvis, I., 1995. High-resolution chemostratigraphy of Quaternary distal turbidites: a case study of new methods for the analysis and correlation of barren sequences. In: Dunay, R.E., Hailwood, E.A. (Eds.), Non-biostratigraphical methods of dating and correlation. Geological Society of London, Bath, pp. 107–143.

Pearce, M.A., Jarvis, I., Swan, A.R.H., Murphy, A.M., Tocher, B.A., Edmunds, W.M., 2003. Integrating palynological and geochemical data in a new approach to palaeoecological studies: Upper Cretaceous of the Banterwick Barn Chalk borehole, Berkshire, UK. Mar. Micropaleontol. 47, 271–306.

Pearce, M.A., Jarvis, I., Tocher, B.A., 2009. The Cenomanian–Turonian boundary event, OAE2 and palaeoenvironmental change in epicontinental seas: New insights from the dinocyst and geochemical records. Palaeogeogr. Palaeoclimatol. Palaeoecol. 280, 207–234.

Pearce, M.A., Lignum, J.S., Jarvis, I., 2011. Senoniasphaera turonica (Prossl, 1990 ex Prossl, 1992) comb. nov., senior synonym of Senoniasphaera rotundata alveolata Pearce et al., 2003: an important dinocyst marker for the Lower Turonian chalk of NW Europe. J. Micropalaentol. 30, 91–93.

Peeters, F.J.C., Hoek, R.P., Brinkhuis, H., Wilpshaar, M., de Boer, P.L., Krijgsman, W., Meulenkamp, J.E., 1998. Differentiating glacio-eustacy and tectonics; a case study involving dinoflagellate cysts from the Eocene–Oligocene transition of the Pindos Foreland Basin (NW Greece). Terra Nova 10, 245–249.

Peleo-Alampay, A.M., Mead, G.A., Wei, W., 1999. Unusual Oligocene Braarudosphaera-rich layers of the South Atlantic and their paleoceanographic implications. J. Nannoplankton Res. 21, 17–26.

Posamentier, H.W., Allen, G.P., 1999. Siliciclastic sequence stratigraphy – concepts and applications. SEPM Concepts Sedimentol. Paleontol 7 (210 pp.).

Poulsen, C.J., Barron, E.J., Johnson, C.C., Fawcett, P., 1999. Links between major climatic factors and regional oceanic circulation in the mid-Cretaceous. In: Barrera, E., Johnson, C.C. (Eds.), Evolution of the Cretaceous Ocean-Climate System. The Geological Society of America, Boulder, pp. 73–89.

Powell, A.J., Dodge, J.D., Lewis, J., 1990. Late Neogene to Pleistocene palynological facies of the Peruvian continental margin upwelling, Leg 112. In: Suess, E., von Huene, R., Emeis, K.-C., Bourgois, J., Cruzado Castañeda, J.d.C, De Wever, P., Eglinton, G., Garrison, R., Greenberg, M., Paz, E.H., Hill, P., Ibaraki, M., Kastner, M., Kemp, A.E.S., Kvenvolden, K., Langridge, R., Lindsley-Griffin, N., Marsters, J., Martini, E., McCabe, R., Ocola, L., Resig, J., Sanchez Fernandez, A.W., Schrader, H.J., Thornburg, T., Wefer, G. (Eds.), Peru Continental Margin. Ocean Drilling Program, College Station TX, pp. 297–321.

Prauss, M., 1993. Sequence-palynology - Evidence from Mesozoic sections and conceptual framework. N. Jb. Geol. Paläont. (Abh.) 190, 143–163.

Prauss, M., 1996. The Lower Toarcian Posidonia-Shale of Grimmen, Northeast Germany. Implications from the palynological analysis of a near-shore section. Neues Jb. Geol. Paläontol. Abh. 200, 107–132.

Prauss, M., 2000. The oceanographic and climatic interpretation of marine palynomorph phytoplankton distribution from Mesozoic, Cenozoic and Recent sections. Göttinger Arbeiter Geol. Paläontol 75, 1–235.

Prauss, M., 2001. Sea-level changes and organic-walled phytoplankton response in a Late Albian epicontinental setting, Lower Saxony basin, NW Germany. Palaeogeogr. Palaeoclimatol. Palaeoecol. 174, 221–249.

Prauss, M., 2006. The Cenomanian/Turonian Boundary Event (CTBE) at Wunstorf, northwest Germany, as reflected by marine palynology. Cretac. Res. 27, 872–886.

Prince, I.M., Jarvis, I., Tocher, B.A., 1999. High-resolution dinoflagellate cyst biostratigraphy of the Santonian–basal Campanian (Upper Cretaceous): new data from Whitecliff, Isle of Wight, England. Rev. Palaeobot. Palynol. 105, 143–169.

Prince, I.M., Jarvis, I., Pearce, M.A., Tocher, B.A., 2008. Dinoflagellate cyst biostratigraphy of the Coniacian–Santonian (Upper Cretaceous): new data from the English Chalk. Rev. Palaeobot. Palynol. 150, 59–96.

Pross, J., 2001. Paleo-oxygenation in Tertiary epeiric seas: evidence from dinoflagellate cysts. Palaeogeogr. Palaeoclimatol. Palaeoecol. 166, 369–381.

Pross, J., Link, E., Ruf, M., Aigner, T., 2006. Delineating sequence stratigraphic patterns in deeper ramp carbonates: quantitative palynofacies data from the Upper Jurassic (Kimmeridgian) of Southwest Germany. J. Sediment. Res. 76, 524–538.

Renard, M., Rafélis, M.d., Emmanuel, L., Beltran, C., Moullade, M., Tronchetti, G., 2007. Fluctuations of sea-water chemistry during Gargasian (Middle Aptian) time. Data from trace-element content (Mg, Sr, Mn, Fe) in hemipelagic carbonates from La Marcouline Quarry (Cassis, SE France). Carnets Géol. 2007/03, 1–28.

Rodríguez-López, J.P., Melendez, N., De Boer, P.L., Rosa Soria, A., 2008. Aeolian sand sea development along the mid-Cretaceous western Tethyan margin (Spain): erg sedimentology and palaeoclimate implications. Sedimentology 55, 1253–1292.

Roelandts, I., Duchesne, J.C., 1994. 1993 compilation of data on five Belgian sedimentary rock reference materials: AWI-1, SBO-1, PRI-1, CCH-1 and DWA-1. Geostand. Newslett. 18, 143–184.

Sageman, B.B., Singer, B.S., Meyers, S.R., Siewert, S.E., Walaszczyk, I., Condon, D.J., Jicha, B.R., Obradovich, J.D., Sawyer, D.A., 2014. Integrating ^{40}Ar/^{39}Ar, U-Pb, and astronomical clocks in the Cretaceous Niobrara Formation, Western Interior Basin, USA. GSA Bull. 126, 956–973.

Schiøler, P., Brinkhuis, H., Roncaglia, L., Wilson, G.J., 1997. Dinoflagellate biostratigraphy and sequence stratigraphy of the Type Maastrichtian (Upper Cretaceous), ENCI Quarry, The Netherlands. Mar. Micropaleontol. 1, 65–95.

Scholle, P.A., Arthur, M.A., 1980. Carbon isotope fluctuation in Cretaceous pelagic limestones: potential stratigraphic and petroleum exploration tool. AAPG Bull. 64, 67–87.

Siesser, W.G., Bralower, T.J., De Carlo, E.H., 1992. Mid-Tertiary *Braarudosphaera*-rich sediments on the Exmouth Plateau. Proc. Ocean Drill. Program Sci. Results 122, 653–663.

Sluijs, A., Pross, J., Brinkhuis, H., 2005. From greenhouse to icehouse; organic-walled dinoflagellate cysts as paleoenvironmental indicators in the Paleogene. Earth-Sci. Rev. 68, 281–315.

Stover, L.E., Hardenbol, J., 1994. Dinoflagellates and depositional sequences in the Lower Oligocene (Rupelian) Boom Clay Formation, Belgium. Bull. Soc. belg. Géol. 102, 5–77.

Stover, L.E., Brinkhuis, H., Damassa, S.P., Verteuil, L.D., Helby, R.J., Monteil, E., Partridge, A.D., Powell, A.J., Riding, J.B., Smelror, M., Williams, G.L., 1996. Mesozoic–Tertiary dinoflagellates, acritarchs and prasinophytes. In: Jansonius, J., McGregor, D.C. (Eds.), Palynology: Principles and Applications (Volume 2). American Association of Stratigraphic Palynologists Foundation, College Station TX, pp. 641–750.

Susek, E., Zonneveld, K.A.F., Fischer, G., Versteegh, G.J.M., Willems, H., 2005. Organic-walled dinoflagellate cyst production in relation to upwelling intensity and lithogenic influx in the Cape Blanc region (off north-west Africa). Phycol. Res. 53, 97–112.

Švábenická, L., 1999. *Braarudosphaera*-rich sediments in the Turonian of the Bohemian Cretaceous Basin, Czech Republic. Cretac. Res. 20, 773–782.

Tappan, H., Loeblich, A.R.J., 1972. Fluctuating rates of protistan evolution, diversification and extinction. Proceedings of the 24th International Geological Congress, Montea, Quebec, pp. 205–213.

Tocher, B.A., 1984. Palynostratigraphy of Uppermost Albian to Basal Coniacian (Cretaceous) Sediments of the Western Anglo-Paris Basin. unpublished PhD thesis, Department of Geology, CNAA, City of London Polytechnic, London, UK, 228 p.

Uličný, D., 2001. Depositional systems and sequence stratigraphy of coarse-grained deltas in a shallow-marine, strike-slip setting: the Bohemian Cretaceous Basin, Czech Republic. Sedimentology 48, 599–628.

Uličný, D., Hladíková, J., Hradecká, L., 1993. Record of sea-level changes, oxygen depletion and the δ^{13}C anomaly across the Cenomanian–Turonian boundary, Bohemian Cretaceous Basin. Cretac. Res. 14, 211–234.

Uličný, D., Laurin, J., Čech, S., 2009. Controls on clastic sequence geometries in a shallow-marine, transtensional basin: the Bohemian Cretaceous Basin, Czech Republic. Sedimentology 56, 1077–1141.

Uličný, D., Jarvis, I., Gröcke, D.R., Čech, S., Laurin, J., Olde, K., Trabucho-Alexandre, J., Švábenická, L., Pedenychouk, N., 2014. A high-resolution carbon-isotope record of the Turonian stage correlated to a siliciclastic basin fill: Implications for mid-Cretaceous sea-level change. Palaeogeogr. Palaeoclimatol. Palaeoecol. 405, 42–58.

Uramoto, G.-I., Tahara, R., Sekiya, T., Hirano, H., 2013. Carbon isotope stratigraphy of terrestrial organic matter for the Turonian (Upper Cretaceous) in northern Japan: Implications for ocean-atmosphere delta C-13 trends during the mid-Cretaceous climatic optimum. Geosphere 9, 355–366.

USGS, 1995a. Certificate of analysis, Cody shale, SCo-1. United States Geological Survey, Denver (p. http://crustal.usgs.gov/geochemical_reference_standards/codyshale.html.).

USGS, 1995b. Certificate of analysis, Diabase, W-2. United States Geological Survey, Denver (p. http://crustal.usgs.gov/geochemical_reference_standards/diabase.html.).

USGS, 1995c. Certificate of analysis, marine sediment, MAG-1. United States Geological Survey, Denver (p. http://crustal.usgs.gov/geochemical_reference_standards/marine.html.).

USGS, 1998. Preliminary certificate of analysis, Andesite, AGV-2. United States Geological Survey, Denver (p. http://crustal.usgs.gov/geochemical_reference_standards/andesite2.html.).

USGS, 2001. Certificate of analysis, Green River shale, SGR-1. United States Geological Survey, Denver (p. http://crustal.usgs.gov/geochemical_reference_standards/shale.html.).

Valečka, J., Skoček, V., 1991. Late Cretaceous lithoevents in the Bohemian Cretaceous Basin, Czechoslovakia. Cretac. Res. 12, 561–577.

Valentine, J.W., 1973. Evolutionary Ecology of the Marine Biosphere. Prentice-Hall, Englewood Cliff NJ (511 pp.).

Voigt, S., 2000. Cenomanian–Turonian composite δ^{13}C curve for Western and Central Europe: the role of organic and inorganic carbon fluxes. Palaeogeogr. Palaeoclimatol. Palaeoecol. 160, 91–104.

Voigt, S., Hilbrecht, H., 1997. Late Cretaceous carbon isotope stratigraphy in Europe: correlation and relations with sea level and sediment stability. Palaeogeogr. Palaeoclimatol. Palaeoecol. 134, 39–59.

Voigt, S., Wiese, F., 2000. Evidence for Late Cretaceous (Late Turonian) climate cooling from oxygen-isotope variations and palaeobiogeographic changes in Western and Central Europe. J. Geol. Soc. Lond. 157, 737–743.

Voigt, S., Gale, A.S., Flogel, S., 2004. Midlatitude shelf seas in the Cenomanian–Turonian greenhouse world: Temperature evolution and North Atlantic circulation. Paleoceanography 19 (art. no.-PA4020.).

Wall, D., 1965. Modern hystrichospheres and dinoflagellate cysts from the Woods Hole region. Grana Palynol.; an intern. J. Palynol. 6, 297–314.

Wall, D., Dale, B., Lohmann, G.P., Smith, W.K., 1977. The environment and climatic distribution of dinoflagellate cysts in modern marine sediments from regions in the North and South Atlantic Oceans and adjacent seas. Mar. Micropaleontol. 2, 121–200.

Wedepohl, K.H., 1971. Environmental influences on the chemical composition of shales and clays. In: Ahrens, L.H., Press, F., Runcorn, S.K., Urey, H.C. (Eds.), Physics and Chemistry of the Earth. Pergamon, Oxford, pp. 307–333.

Wiese, F., 1999. Stable isotope data (δ^{13}C, δ^{18}O) from the Middle and Upper Turonian (Upper Cretaceous) of Liencres (Cantabria, northern Spain) with a comparison to northern Germany (Söhlde & Salzgitter-Salder). Newsl. Stratigr. 37, 37–62.

Wiese, F., Voigt, S., 2002. Late Turonian (Cretaceous) climate cooling in Europe: faunal response and possible causes. Geobios 35, 65–77.

Wilpshaar, M., Leereveld, H., 1994. Palaeoenvironmental change in the Early Cretaceous Vocontian Basin (SE France) reflected by dinoflagellate cysts. Rev. Palaeobot. Palynol. 84, 121–128.

Zevenboom, D., Brinkhuis, H., Visscher, H., 1994. Dinoflagellate cyst palaeoenvironmental analysis of the Oligocene / Miocene transition in northwest and central Italy. Giornale di Geologia Serie 3a 56, 155–169.